A Local Wave Tracking Strategy for Efficiently Solving Mid- and High-Frequency Helmholtz Problems

Mohamed Amara, Sharang Chaudry, Julien Diaz, Rabia Djellouli, Steven Fiedler

A Local Wave Tracking Strategy for Efficiently Solving Mid- and High-Frequency Helmholtz Problems

Mohamed Amara, Sharang Chaudry, Julien Diaz, Rabia Djellouli, Steven Fiedler

RESEARCH REPORT

N° 8364

September 2013

Project-Teams Magique 3D

ISSN 0249-6399 ISRN INRIA/RR--8364--FR+ENG

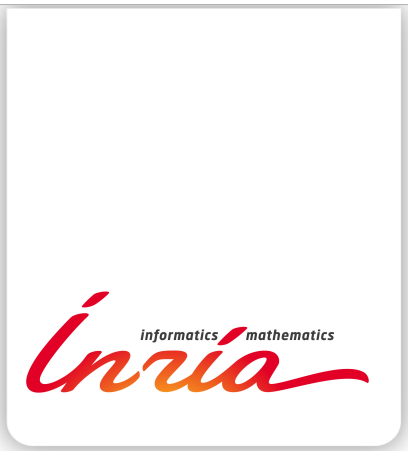

A Local Wave Tracking Strategy for Efficiently Solving Mid- and High-Frequency Helmholtz Problems

Mohamed Amara[*†], Sharang Chaudry[‡], Julien Diaz[§¶], Rabia Djellouli[‖], Steven Fiedler[** ††]

Project-Teams Magique 3D

Research Report n° 8364 — September 2013 — 47 pages

[*] LMA/CNRS UMR 5142, Université de Pau et des Pays de l'Adour, France.
[†] INRIA Bordeaux Sud-Ouest Research Center, Team Project Magique-3D, France.
[‡] Interdisciplinary Research Institute for the Sciences (IRIS) and Department of Mathematics. California State University, Northridge, Northridge, California, USA
[§]
[¶]
[‖]
[**]
[††] Department of Chemistry, Pomona College, Claremont, California, USA

RESEARCH CENTRE
BORDEAUX – SUD-OUEST

200 avenue de la Vieille Tour
33405 Talence Cedex

Abstract: We propose a procedure for selecting basis function orientation to improve the efficiency of solution methodologies that employ local plane-wave approximations. The proposed adaptive approach consists of a local wave tracking strategy. Each plane-wave basis set, within considered elements of the mesh partition, is individually or collectively rotated to best align one function of the set with the local propagation direction of the field. Systematic determination of the direction of the field inside the computational domain is formulated as a minimization problem. As the resultant system is nonlinear with respect to the directions of propagation, the Newton method is employed with exact characterization of the Jacobian and Hessian. To illustrate the salient features and evaluate the performance of the proposed wave tracking approach, we present error estimates as well as numerical results obtained by incorporating the procedure into a prototypical plane-wave based approach, the least-squares method (LSM) developed by Monk et al. [29]. The numerical results obtained for the case of a two-dimensional rigid scattering problem indicate that (a) convergence was achievable to a prescribed level of accuracy, even upon initial application of the tracking wave strategy outside the pre-asymptotic convergence region, and (b) the proposed approach reduced the size of the resulting system by up to two orders of magnitude, depending on the frequency range, with respect to the size of the standard LSM system.

Key-words: direct scattering, domain decomposition, Helmholtz equation, Newton method, finite element method, pollution effect, adaptive direction, plane-wave-based method, least-squares method

Méthodes d'ondes planes adaptatives pour la résolution efficace de problèmes de Helmholtz à moyenne et haute fréquence

Résumé : Nous proposons une technique permettant d'optimiser l'orientation des fonctions de base pour améliorer la précision des méthodes basées sur des approximations par ondes planes. Cette approche repose une stratégie adaptative locale des ondes planes et consiste à appliquer des rotations aux bases d'ondes planes, individuellement ou par groupe d'élément d'une même partition, de manière à les aligner au mieux avec la direction de propagation du champ d'onde. La détermination de ces directions de propagation est effectué en résolvant un problème de minimisation. Le système qui en découle étant non linéaire par rapport aux directions de propagations, nous utilisons la méthode de Newton en calculant le Jacobien et le Hessien de manière exacte. Nous présentons des estimations d'erreur et des résultats numériques permettant d'illustrer les principales propriétés et d'évaluer les performances de la méthode. Pour cela, nous avons mis en œuvre la stratégie adaptative dans un code numérique basé sur approche par ondes planes classiques, la méthode des moindres carrés (Least Squares Method, LSM), développée par Monk et al. [29]. Les résultats numériques obtenus pour le problème de diffraction en dimension deux mettent en évidence que la méthode (a) converge pour un niveu de précision donné, même si la stratégie adaptative est utilisée en dehors de la région de convergence préasymptotique ; et (b) la méthode réduit la taille du système linéaire jusqu'à deux ordres de magnitude suivant la fréquence choisie par rapport à la LSM classique.

Mots-clés : diffraction, décomposition de domaine, équation d'Helmholtz, méthode de Newton, méthode d'élements finis, effets de pollution, direction adaptative, méthode d'ondes planes, méthodes des moindres carrés

1 Introduction

Use of wave equations to model physical phenomena is well documented with wide-ranging application in optics [2], seismology [1], radar [14], and ocean acoustics [33], along with many other fields in science and technology. While the ubiquitous finite element method has served as a foundation for the solution of this class of equations, issues that arise from the frequency dependence of the discretization, identified as a pollution effect [5, 13], have remained a topic of active research for over a half a century. Many attempts have been made to overcome the difficulties related to this pollution effect. Relatively recently, approaches that employ plane-waves as basis functions for Helmholtz problems have demonstrated significant potential to numerically determine these solutions [34, 4, 8, 29, 12, 21, 22, 26, 27, 18, 19, 20, 15, 17, 16, 3]. The oscillatory nature of plane-waves provides a natural setting to more efficiently model highly oscillatory fields. Nevertheless, fields that propagate with a high frequency remain difficult to compute, due to an increasing presence of numerical instabilities created upon refined discretization and/or the augmentation of the basis sets with additional plane-wave functions. These instabilities arise due to the numerical loss of linear independence of functions within the basis sets, as observed and demonstrated in [3, 24].

In response to the above numerical challenges, we propose an alternative procedure that can extend the range of satisfactory convergence without significantly increasing the number of plane-waves and/or drastically refining the mesh. This can mitigate the nascent presence of near-linear dependencies that instigate numerical breakdown. The essence of the proposed approach is to maintain a low number of plane-waves typically used to calculate fields propagating in the low frequency regime, to calculate fields at higher frequencies. This is accomplished by allowing the elemental basis sets to rotate so as to align a basis function in the set, with the main direction of field propagation. In this manner, a more accurate approximation of the field is expected to that obtained by rigid, and often arbitrarily predefined orientations of the basis sets. The proposed approach, which can be viewed as an adaptive-type strategy, is succinctly demonstrated by comparison of the analytical to the numerical solution for a plane-wave propagating at an angle θ through a square waveguide domain of length a [9]. In the domain, a high frequency propagation is considered (ka=500), with the wavenumber represented by k. Using a basis set of four canonically oriented plane-waves per element, over 100% relative error was determined with the Least-Squares Method (LSM) [29] for a step-size h/a=1/100 for all propagation angles except those aligned with the predefined basis functions ($0°, 90°, 180°$ and $270°$), as depicted in Fig. 1. However, if the basis functions were allowed to rotate so that one function within an element aligns with the direction of propagation of the field, the "rotated" LSM delivered an error of 10^{-6}% with a much larger step size: h/a=1/2, corresponding to a mesh partition of only two elements. Note that the same degree of rotation was applied to each of the four basis sets, a logical option due to the common directions of propagation through each element. In effect, allowing the basis functions to align, or track the direction of propagation of the field within a given element, improved the calculation accuracy, while mitigating discretization cost by a factor of 2500 in the case of the considered waveguide problem. We subsequently will refer to this wave tracking (WT) method as LSM-WT in this study.

The above example is simple; it contains one direction of propagation, whereas realistic objects generate scattered fields with multiple directions of propagation. In this paper, we propose an approach to permit the basis functions to rotate and systematically track the local direction of field propagation. In this manner, the method can numerically solve direct scattering problems in domains containing fields with multiple directions of propagation. To this end, the proposed

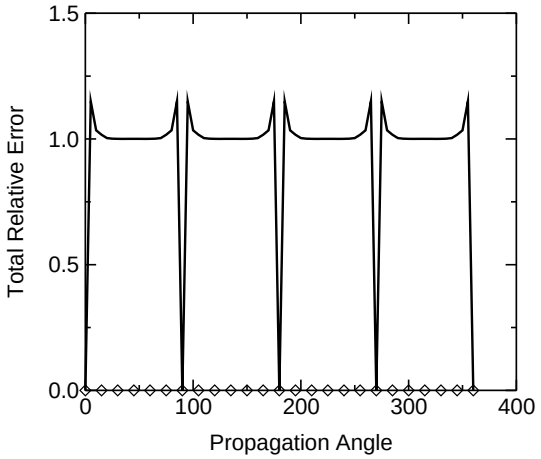

Figure 1: Sensitivity of the relative error to the angle of propagation for $ka = 500$ and 4 plane-waves: LSM with $h/a = 1/100$ (line) and LSM-WT with $h/a = 1/2$ (diamond symbols).

approach represents the scattered field at the element level by a superposition of plane-waves, where both the expansion coefficients (the nodes) and angles of orientation are unknown and need to be determined. Computation of these unknowns can be expressed as a double minimization problem, which is linear with respect to the nodes and non-linear with respect to the determination of the angles of orientation of the basis functions. In this study, the Newton iterative method was employed to address the nonlinear aspect of the formulation, although other methods can be employed, e.g., conjugate gradient and genetic algorithms, [23, 11]. The resulting, smaller, linear systems corresponding to the scattering problem and Newton iteration equations are solved by LU factorization. Although solution of the double minimization problem appears to require determination of an increased number of unknowns, in point of fact, the proposed WT formalism incurs a significantly smaller size than required by existing methods, as a coarser mesh and lower number of basis functions are needed for a given level of accuracy. This effectively raises the onset of numerical instabilities that arise from near-linear dependencies of the basis set functions at higher frequencies. Consequently, the WT approach is designed to enhance convergence stability and reduce computational cost. Both factors can, in turn, extend the accessible range for the application of plane-wave based solution methodologies to higher frequency scattering problems.

It should be emphasized that the proposed wave-tracking procedure is general and can be incorporated into plane-wave based formulations that lead to minimization of a cost function. To exemplify application, the algorithm, delineated in Sec. 3.1, is developed in this study in conjunction with LSM (Sec. 3.2). The accuracy and efficiency of the resultant LSM-WT method is assessed for a prototypical scattering problem consisting of a sound-hard disk-shaped scatterer embedded in a circular computational domain (Sec. 5). The calculated scattered acoustic field is subsequently compared to the field generated by the (unmodified) LSM. Accuracies of the approximated fields obtained by LSM and LSM-WT are compared by calculating the relative error in an H^1-type norm. The proposed approach is found to converge to a prescribed level of accuracy, even upon initial application of the Newton algorithm outside the pre-asymptotic

convergence region. The required size of the scattering system is reduced with LSM-WT by one and two-orders of magnitude, depending on the frequency range with respect to the standard LSM system. Analysis of the resultant orientational angles reveal that significant, independent, basis set rotations are required to achieve the targeted error thresholds. This indicates that a) optimal orientaion angles can not be predicted a priori, and b) a straightforward, sweeping approach would be ineffective, due to exorbitant computational cost.

2 Preliminaries

To assess the performance of the proposed strategy, we consider the following prototypical Helmholtz problem: direct acoustic scattering from a sound-hard object in the presence of an artificial exterior boundary, Σ, as shown in Fig. 2. However, the wave-tracking procedure can accommodate other interior [10] as well as other exterior boundary conditions (see e.g., Refs. [39, 7] and references therein). The scattered field, u, is then the unique solution of the boundary value problem:

$$\text{(BVP)} \quad \begin{cases} \Delta u + k^2 u &= 0 & \text{in } \Omega, \\ \partial_n u &= g & \text{on } \Gamma, \\ \partial_n u &= \mathrm{i}ku & \text{on } \Sigma, \end{cases} \tag{1}$$

where Ω is a two-dimensional computational domain, ∂_n is the normal derivative operator evaluated on the respective boundaries, Γ and Σ, k is a positive number representing the wavenumber, and g is a complex-valued function. A standard example of such a function is given by:

$$g(\vec{x}) = -\partial_n e^{\mathrm{i}k\vec{x}\cdot\vec{d}} \tag{2}$$

where $\vec{d}$ is a unit vector representing the direction of the incident plane-wave. To numerically approximate the scattered field, the computational domain, Ω, is partitioned into a regular triangulation $\mathcal{T}_h$ of N_h quadrilateral- or triangular-shaped elements, K:

$$\Omega = \bigcup_{j=1}^{N_h} K_j. \tag{3}$$

Assume that solution of the BVP, given in Eq. (1), by plane-wave-based variational methods can be formulated to be compactly expressed as a minimization of a cost function J:

$$\begin{cases} \text{Find } u_h \in X_h \text{ such that,} \\ J(u_h) = \inf\limits_{v \in X_h} J(v), \end{cases} \tag{4}$$

with the global space X_h defined by:

$$X_h \;=\; \left\{ v \in L^2(\Omega);\; \middle|\; \forall K \in \mathcal{T}_h,\; v_{|_K} = v^K \in X_h(K) \right\}. \tag{5}$$

where element $K \in \mathcal{T}_h$ possesses n^K basis functions. Hence, the local subspaces $X_h(K) \subseteq H^1(K)$ are given by:

$$X_h(K) \;=\; \left\{ v^K : K \to \mathbb{C} \;\middle|\; v^K \;=\; \sum_{j=1}^{n^K} \xi_j^K \phi_j^K; \quad \text{where } \xi_j^K \in \mathbb{C} \right\}, \tag{6}$$

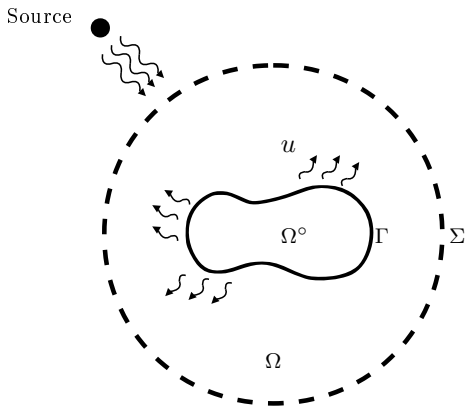

Figure 2: Sample computational domain for the scattering problem.

where:

$$\phi_j^K(\vec{x}) \;=\; e^{\mathrm{i}k\,\vec{d}_j^K\cdot(\vec{x}-\vec{x}^K)}; \quad 1\le j\le n^K;\ \vec{x}\in K, \tag{7}$$

with $\vec{x}^K$ as the centroid of K, and $\vec{d}_j^K$ as the direction of the propagation of the plane-waves, i.e., $\vec{d}_j^K = (\cos\theta_j, \sin\theta_j)$. The set of angles $\{\theta_j\}$ is such that $\theta_j \in [0, 2\pi)$ and $\theta_j \neq \theta_l$ if $j \neq l$. For example,

$$\theta_j = 2\pi(j-1)/(n^K-1)\ ; 1\le j\le n^K.$$

3 Solution Methodology

3.1 The general tracking wave strategy

The proposed wave-tracking approach guides a set of local basis functions to align one function closely with the orientation of the local (intra-element) propagation of the field, u. To this end, an adaptive strategy is employed by which the direction of the initial choice of the local basis functions are rotated within each element or an ensemble of elements, by employing a rotational matrix, $\mathbf{R}_\alpha$; for the following rotation in $\mathbb{R}^2$,

$$\mathbf{R}_\alpha(\vec{x}) = \begin{bmatrix}\cos\alpha & -\sin\alpha\\ \sin\alpha & \cos\alpha\end{bmatrix}\begin{bmatrix}x_1\\ x_2\end{bmatrix}; \alpha\in[0,2\pi), \tag{8}$$

with the angle of rotation, α, employed to best align one function in the basis set with the direction of field propagation. For each element, K, and angle, α^K, we define a new set of basis functions $\left(\psi_j^K(\alpha^K)\right)_{j=1,\cdots,n^K}$ by rotating the considered plane-waves $\left(\phi_j^K\right)_{j=1,\cdots,n^K}$ through the angle α^K, as illustrated in Fig.3.

$$\psi_j^K(\alpha^K)(\vec{x}) = \phi_j^K(\mathbf{R}_{\alpha^K}(\vec{x}))\ ;\ j=1,\cdots,n^K,\ \forall K\in\mathcal{T}_h. \tag{9}$$

Note that the resulting basis functions ψ_j^K are also plane-waves that satisfy the Helmholtz equation in $\mathbb{R}^2$. The resulting field, u_h, which accommodates an arbitrary angle of field propagation, θ_j, is defined at the element level as,

$$u_h(\vec{\alpha})|_K = \sum_{j=1}^{n^K}\xi_j^K(\alpha^K)\ e^{ik\vec{d}_j(\alpha^K)\cdot(\vec{x}-\vec{x}^K)}\ ;\ \forall K\in\mathcal{T}_h, \tag{10}$$

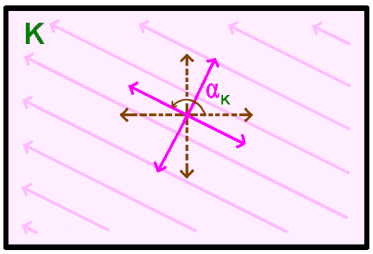

Figure 3: Basis set rotation to align one basis function with the direction of propagation in element, K: Initial basis set (dashed line), final orientation (solid line) with counterclockwise rotational angle given by α^K.

where the new orientations are obtained by a counterclockwise rotation by angle α^K, that is:

$$\vec{d}_j(\alpha^K) = (\cos(\theta_j + \alpha^K), \sin(\theta_j + \alpha^K)). \tag{11}$$

Note that the unknown expansion coefficients, ξ_j^K, now also depend on the unknown angle, α^K. Globally, the field is defined across the computational domain as:

$$u_h(\vec{\alpha}) = \sum_{K \in \mathcal{T}_h} u_h(\alpha^K)|_K \, \chi|_K \tag{12}$$

where $\chi|_K$ being the characteristic function of K. Note that the total number of basis functions specified is $N_\phi = n^K \times N_h$. The minimization problem defined in Eq. (4) is reformulated using the new, rotated, basis functions given by Eq. (9). In this manner, the original minimization problem given by Eq. (4) becomes a double minimization consisting of finding a vector angle $\vec{\theta}$ such that:

$$\begin{cases} \text{Find } \vec{\theta} \in \mathcal{D}_h \text{ and } u_h(\vec{\theta}) \in \hat{X}_h(\vec{\theta}) \text{ such that,} \\ J(u_h(\vec{\theta})) \;=\; \inf\limits_{\vec{\alpha} \in \mathcal{D}_h} \inf\limits_{v \in \hat{X}_h(\vec{\alpha})} J(v), \end{cases} \tag{13}$$

where $\mathcal{D}_h$ is the space corresponding to all possible directions of propagation of the field in the domain Ω:

$$\mathcal{D}_h = \left\{ \vec{\alpha} \in L^2(\Omega); \forall\, K \in \mathcal{T}_h,\ \alpha_{|_K} = \alpha^K \ \in [0, 2\pi) \right\}, \tag{14}$$

the modified global discrete space $\hat{X}_h(\vec{\alpha}) \subseteq L^2(\Omega)$ as:

$$\hat{X}_h(\vec{\alpha}) \;=\; \left\{ v \in L^2(\Omega); \forall\, K \in \mathcal{T}_h,\ v_{|_K} = v^K \in \hat{X}_h(K, \alpha^K) \right\}, \tag{15}$$

$\vec{\alpha}$ is a given vector in $\mathbb{R}^{N_h}$, with coordinates defined as the rotational angle for each element K. The local subspaces $\hat{X}_h(K, \theta^K) \subseteq H^1(K)$ are defined by:

$$\hat{X}_h(K, \alpha^K) \;=\; \left\{ v^K : K \to \mathbb{C}\ ;\ v^K = \sum_{j=1}^{n^K} \xi_j^K \psi_j^K(\alpha^K)\ ; \quad \text{where } \ \xi_j^K \in \mathbb{C} \right\}. \tag{16}$$

We may choose an exhaustive approach to track at the element level as indicated in $\mathcal{D}_h$, however, it is preferable from the standpoint of computational efficiency to use a priori knowledge or an

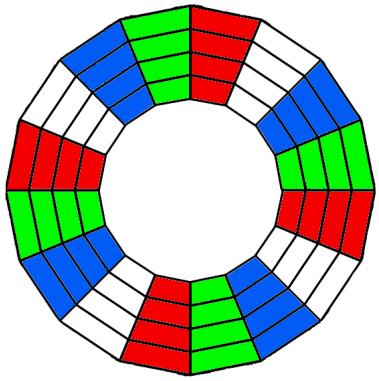

Figure 4: Disk-shaped scatterer: Example of a mesh comprised as a 16-sided regular polygon with 4 radial and 16 angular elements. Angularly adjacent elements are grouped into a given subdomain, specified by color and assigned a common angle of orientation. Subdomains are shown as replicated in each quadrant.

adaptive strategy to determine regions with similar directions of field propagation, and stipulate a common basis set orientation for elements in these regions. Such an approach will lead to a significant computational cost reduction, as demonstrated in the following. The computational domain, Ω, is partitioned into N_Ω subdomains. Denoting $\{\Omega_\mu\}$ as the set of subdomains that posses elements with a common direction field propagation:

$$\Omega = \bigcup_{\mu=1}^{N_\Omega} \Omega_\mu, \tag{17}$$

where:

$$\Omega_\mu = \bigcup_{j=1}^{n_h^\mu} K_j; \quad \mu = 1, 2, \ldots, N_\Omega, \tag{18}$$

with n_h^μ elements K per subdomain, Ω_μ (see Fig. 4 for an illustrative example with 4 elements per subdomain, and 4 subdomains per quadrant). The double minimization problem, given by Eq. (13), is re-formulated as follows:

$$\begin{cases} \text{Find } \vec{\theta} \in \widetilde{\mathcal{D}}_h \text{ and } u_h(\vec{\theta}) \in \hat{X}_h(\vec{\theta}) \text{ such that,} \\ J(u_h(\vec{\theta})) \;=\; \inf\limits_{\vec{\alpha}\in\widetilde{\mathcal{D}}_h} \inf\limits_{v\in\hat{X}_h(\vec{\alpha})} J(v), \end{cases} \tag{19}$$

with $\widetilde{\mathcal{D}}_h \subseteq \mathcal{D}_h$, such that $\widetilde{\mathcal{D}}_h = \left\{\vec{\alpha} \in \mathcal{D}_h;\ \alpha|_{\Omega_\mu} = \alpha_\mu \in [0, 2\pi)\right\}$. Hence, $\vec{\theta}$ is a vector in $\mathbb{R}^{N_\Omega}$, where $N_\Omega << N_h$, and N_h is the number of elements given by Eq. (3). The double minimization Eq. (19), can be compacted to avoid unnecessary complexity in the notation:

$$J(u_h(\vec{\theta})) \;=\; \inf_{\vec{\alpha}\in\widetilde{\mathcal{D}}_h} L(\vec{\alpha}) \tag{20}$$

with the cost function L defined as:

$$L(\vec{\alpha}) \;=\; \inf_{v\in\hat{X}_h(\vec{\alpha})} J(v). \tag{21}$$

For clarity and later reference, we also set:

$$L_h \;=\; \inf_{\vec{\alpha}\in\widetilde{\mathcal{D}}_h} L(\vec{\alpha}). \tag{22}$$

Solving the double minimization problem given by Eqs. (21)-(22), requires application of a descent method or other optimization approaches such as the conjugate gradient method [23] or a genetic algorithm [11]. We propose to determine this minimum by seeking the roots of the Jacobian operator, denoted by $\vec{\dot{L}}(\vec{\alpha})$. In this study, the Newton method is employed to determine the resulting non-linear system. This algorithm incurs at iteration, m, the Newton iteration equation:

$$\ddot{\mathbf{L}}(\vec{\alpha}^{\,(m)})\delta\vec{\alpha}^{\,(m)} = -\vec{\dot{L}}(\vec{\alpha}^{\,(m)}) \tag{23}$$

with $\ddot{\mathbf{L}}$ as the Hessian, and $\delta\vec{\alpha}$ as the angular update. The solution of the linear system specified in Eq. (23), yield the set of angular updates $\delta\vec{\alpha}^{(m)}$. For each iteration, m, the update is then applied to the set of basis functions:

$$\vec{\alpha}^{(m+1)} = \vec{\alpha}^{(m)} + \delta\vec{\alpha}^{(m)}. \tag{24}$$

3.2 Wave tracking formulation as applied to the least-squares method

The following delineates the formulation of the proposed wave-tracking strategy in conjunction with the least squares approach [29].

3.2.1 Pertinent LSM formalism

In this study, we apply the general wave-tracking formalism defined in the previous section, in conjunction with the least-squares method [29]. The cost function, J, given by Eq. (4) in the LSM format takes the form:

$$\begin{aligned} J(v) = \sum_{e:\,\text{interior edge}} \left(\frac{1}{k^2 h_e}\int_e |[v]|^2 ds + \frac{1}{h_e}\int_e |[[\partial_n v]]|^2 ds \right) \\ + \sum_{e\,\subset\Gamma_h\cup\Sigma_h} \frac{1}{k^2 h_e}\int_e |\partial_n v - ik\chi_{\Sigma_h} v - \chi_{\Gamma_h} g|^2 ds \end{aligned} \tag{25}$$

with h_e as the length of edge e, $[v]$ and $[[v]]$ denoting the jump of v across an interior edge of two adjacent elements: $\partial K \cap \partial K'$:

$$\begin{aligned} [v] \;&=\; v|_K - v|_{K'}, \\ [[v]] \;&=\; v|_K + v|_{K'}, \end{aligned} \tag{26}$$

χ_{Γ_h} (resp. χ_{Σ_h}) is the characteristic function of Γ_h (resp. Σ_h), the inner (resp. outer) boundary, and ∂_n is the normal derivative operator evaluated with respect to the edge. The solution of the minimization problem, given by Eq. (4), is then obtained by solving the following Variational Formulation (VF) [29]:

$$\text{(VF)} \quad \left\{ \begin{array}{l} \text{Find } u_h \in V_h \text{ such that :} \\ a(u_h\ ,\ w) \;=\; F(w)\ ;\ \forall w \in V_h, \end{array} \right. \tag{27}$$

where the hermitian bilinear form $a(\cdot,\cdot)$ is given by:

$$\begin{aligned} a(v,w) &= \sum_{e:\,\text{interior edge}} \left(\frac{1}{k^2 h_e} \int_e [[\partial_n v]]\overline{[[\partial_n w]]}\, ds + \frac{1}{h_e}\int_e [v]\overline{[w]}\, ds \right) \\ &+ \sum_{e\,\subset\,\Gamma_h \cup \Sigma_h} \frac{1}{k^2 h_e} \int_e (\partial_n v - \mathrm{i}\, k\chi_\Sigma\, v)(\overline{\partial_n w - \mathrm{i}\, k\chi_\Sigma\, w})\, ds, \end{aligned} \tag{28}$$

and the linear functional F is given by:

$$F(w) \;=\; \sum_{e\subset\Gamma_h} \frac{1}{k^2 h_e} \int_e g\,(\overline{\partial_n w})\, ds;\;\; \forall w \in V_h. \tag{29}$$

Last, the space V_h is a finite dimensional space whose elements w satisfy $\Delta w + k^2\, w = 0$ in K ; $\forall K \in \mathcal{T}_h$.

3.2.2 The LSM-WT Method

In the following, we provide a characterization of the Jacobian, $\vec{\dot{L}}(\vec{\alpha})$, and the Hessian, $\ddot{\mathbf{L}}(\vec{\alpha})$ in the context of the LSM formulation. Recall $\vec{\alpha} \to L(\vec{\alpha})$ is an infinitely differentiable function.

Proposition 3.1. *Let $\alpha \in \mathcal{D}_h$. Then:*

roman zeze*

roman $\vec{\dot{L}}(\vec{\alpha}) \in \mathbb{C}^{N_\Omega}$ and its μ^{th} coordinate, $\dot{L}_\mu(\vec{\alpha})$, satisfies:

$$\dot{L}_\mu(\vec{\alpha}) \;=\; \frac{\partial L(\vec{\alpha})}{\partial \alpha_\mu} \;=\; \frac{1}{2}\sum_{e\subset\Gamma} \int_e \partial_n \dot{u}_{h,\mu}(\vec{\alpha})\, \overline{g}\, ds; \quad \mu = 1,\ldots,N_\Omega, \tag{30}$$

where, $\dot{u}_{h,\mu}(\vec{\alpha})$, the first-order partial derivative of $u_h(\vec{\alpha})$ with respect to angle α_μ, is expressed as follows:

$$\dot{u}_{h,\mu}(\vec{\alpha}) \;=\; \dot{u}^a_{h,\mu}(\vec{\alpha}) \;+\; \dot{u}^b_{h,\mu}(\vec{\alpha}); \quad \mu = 1,\ldots,N_\Omega, \tag{31}$$

with,

$$\dot{u}^a_{h,\mu}(\vec{\alpha}) \;=\; \sum_{K\in\mathcal{T}_h} \sum_{j=1}^{n^K} \dot{\xi}^K_{\mu,j}\, \psi^K_j(\alpha^K), \qquad \dot{u}^b_{h,\mu}(\vec{\alpha}) \;=\; \sum_{K\subset\Omega_\mu} \sum_{j=1}^{n^K} \xi^K_j\, \dot{\psi}^K_{j,\mu}(\alpha^K), \tag{32}$$

and

$$\dot{\psi}^K_{j,\mu}(\alpha^K) = \partial\psi^K_j(\alpha^K)/\partial\alpha_\mu. \tag{33}$$

roman $\ddot{\mathbf{L}}(\vec{\alpha}) \in \mathbb{C}^{N_\Omega \times N_\Omega}$, and its entries, $\ddot{L}_{\mu\mu'}(\vec{\alpha})$, satisfy:

$$\ddot{L}_{\mu\mu'}(\vec{\alpha}) \;=\; \frac{\partial^2 L(\vec{\alpha})}{\partial\alpha_\mu \partial\alpha_{\mu'}} \;=\; \frac{1}{2}\sum_{e\subset\Gamma} \int_e \partial_n \ddot{u}_{h,\mu\mu'}(\vec{\alpha})\overline{g}\, ds; \quad \mu,\mu' = 1,\ldots,N_\Omega, \tag{34}$$

where, $\ddot{u}_{h,\mu\mu'}$, the second-order partial derivative of $u_h(\vec{\alpha})$ with respect to angles α_μ and $\alpha_{\mu'}$, is expressed as follows:

$$\ddot{u}_{h,\mu\mu'}(\vec{\alpha}) \;=\; \ddot{u}^a_{h,\mu\mu'}(\vec{\alpha}) + \ddot{u}^b_{h,\mu\mu'}(\vec{\alpha}) + \ddot{u}^c_{h,\mu\mu'}(\vec{\alpha}); \quad \mu,\mu' = 1,\ldots,N_\Omega, \tag{35}$$

with

$$\begin{aligned}
\ddot{u}^a_{h,\mu\mu'}(\vec{\alpha}) &= \sum_{K\in\mathcal{T}_h}\sum_{j=1}^{n^K} \ddot{\xi}^K_{\mu\mu',j}\,\psi^K_j(\alpha^K),\;\; \ddot{u}^b_{h,\mu\mu'}(\vec{\alpha}) = \sum_{K\subset\Omega_\mu}\sum_{j=1}^{n^K} \dot{\xi}^K_{j,\mu}\dot{\psi}^K_{j,\mu'}(\alpha^K)\\
\ddot{u}^c_{h,\mu\mu'}(\vec{\alpha}) &= \sum_{K\subset\Omega_\mu\cap\Omega_{\mu'}}\sum_{j=1}^{n^K} \xi^K_j\ddot{\psi}^K_{j,\mu\mu'}(\alpha^K),
\end{aligned} \tag{36}$$

and

$$\ddot{\psi}^K_{j,\mu\mu'}(\alpha^K) = \partial^2\psi^K_j(\alpha^K)/\partial\alpha_\mu\partial\alpha_{\mu'}. \tag{37}$$

Proof. The key step to prove Proposition 3.1 is to establish that

$$L(\vec{\alpha}) \;= \frac{1}{2}\sum_{e\subset\Gamma}\frac{1}{k^2h_e}\int_e \partial_n u_h(\vec{\alpha})\,\overline{g}\;ds; \tag{38}$$

This property results from Eqs. (25)-(26) and then applying Green-Riemann to Eq. (25). Then, using the chain rule in Eq. (38) leads to the desired result in (i) and (ii). □

Remark 1. Consideration of the first- and second-order Fréchet derivatives $\dot{u}_h(\alpha)$ and $\ddot{u}_h(\vec{\alpha})$ allows facile determination of the expansion coefficients: $\vec{\xi}$, $\vec{\dot{\xi}}_\mu$, and $\vec{\ddot{\xi}}_{\mu,\mu'}$. The latter are required for construction of the Jacobian $\vec{L}(\vec{\alpha})$, and Hessian, $\ddot{\mathbf{L}}(\vec{\alpha})$ that incur in the Newton iteration equation, given by Eq. (23). Evaluation of the Fréchet derivatives is achieved by solving the same variational problem with different right-hand sides, as demonstrated in the following two results.

Proposition 3.2. *Let $\vec{\alpha}\in\mathcal{D}_h$. Then, $u_h(\vec{\alpha})$, $\dot{u}^a_{h,\mu}(\vec{\alpha})$, and $\ddot{u}^a_{h,\mu\mu'}(\vec{\alpha})$ are solutions of the variational problem:*

$$\text{(VF)}\quad \left\{\begin{array}{l} \text{Find } \tilde{u}_h(\vec{\alpha})\in\hat{X}_h(\vec{\alpha}) \text{ such that :}\\ a(\tilde{u}_h(\vec{\alpha})\;,\;\psi^K_j(\alpha^K)) = \;G(\psi^K_j(\alpha^K))\;; \quad \forall j=1,\cdots n^K,\;\forall K\in\mathcal{T}_h \end{array}\right. \tag{39}$$

where the expression of the linear functional G depends on the sought-after field $\tilde{u}_h(\alpha)$ as follows:

roman. For $\tilde{u}_h(\vec{\alpha}) = u_h(\vec{\alpha})$, we have:*

$$G(\psi^K_j(\alpha^K)) \;=\; F(\psi^K_j(\alpha^K)) \tag{40}$$

where the field $u_h(\vec{\alpha})$ is given by Eq. (10) and the linear functional F is given by Eq. (29).

roman. For $\tilde{u}_h(\vec{\alpha}) = \dot{u}^a_{h,\mu}(\vec{\alpha})$, we have:*

$$G(\psi^K_j(\alpha^K)) = F(\dot{\psi}^K_{j,\mu}(\alpha^K)) - a(u_h(\vec{\alpha}),\dot{\psi}^K_{j,\mu}(\alpha^K)) - a(\dot{u}^b_{h,\mu}(\vec{\alpha}),\psi^K_j(\alpha^K)) \tag{41}$$

where the field $\dot{u}^a_{h,\mu}(\vec{\alpha})$ is given by Eq. (32), the linear functional F is given by Eq. (29), *the bilinear form $a(\cdot,\cdot)$ is given by Eq.* (39), *and $\dot{u}^b_{h,\mu}(\vec{\alpha})$ is given by Eq.* (32).

roman*. *For* $\tilde{u}_h(\vec{\alpha}) = \ddot{u}^a_{h,\mu\mu'}(\vec{\alpha})$, *we have:*

$$\begin{array}{rcl} G(\psi_j^K(\alpha^K)) & = & F(\ddot{\psi}^K_{j,\mu\mu'}(\alpha^K)) - 2a(\dot{u}_{h,\mu}(\vec{\alpha}), \dot{\psi}^K_{j,\mu}(\alpha^K) - a(\dot{u}^b_{h,\mu}(\vec{\alpha}), \ddot{\psi}^K_{j,\mu\mu'}(\alpha^K)) \\ & - & 2a(\ddot{u}^b_{h,\mu\mu'}(\vec{\alpha}), \ddot{\psi}^K_{\mu\mu',j}(\alpha^K)) - a(\ddot{u}^c_{h,\mu\mu'}(\vec{\alpha}), \psi^K_j(\alpha^K)) \end{array} \tag{42}$$

where the fields $\ddot{u}^a_{h,\mu\mu'}(\vec{\alpha})$, $\ddot{u}^b_{h,\mu\mu'}(\vec{\alpha})$ *and* $\ddot{u}^c_{h,\mu\mu'}(\vec{\alpha})$ *are given by Eq.* (36).

Proof. Property (i) results from substituting $w = \psi_j^K(\vec{\alpha})$ in VF (27). To prove property (ii), we consider first Eq. (39) and Eq. (40). We have,

$$a(u_h(\vec{\alpha}), \phi_j^K(\alpha^K) = F(\psi_j(\alpha^K)) \tag{43}$$

We differentiate with respect to α_μ^K and use the fact that $a(\cdot,\cdot)$(resp. F$(\cdot)$) is a bilinear (resp. linear) form. We obtain,

$$a\left(\frac{\partial u_h}{\partial \alpha_\mu}, \psi_j^K(\alpha^K)\right) + a\left(u_h(\vec{\alpha}), \frac{\partial \psi_j^K(\alpha^K)}{\partial \alpha_\mu}\right) = F\left(\frac{\partial \psi_j(\alpha^K)}{\partial \alpha_\mu}\right). \tag{44}$$

Then, substituting Eqs. (31), (32) and (33) in Eq. (44) leads to the desired result given by Eqs. (39) and Eq. (41). The proof of Property (iii) results from applying the second order derivative with respect to α_μ and $\alpha_{\mu'}$ to Eq. (43), and then substituting into the obtained result, the expression of the second order partial derivative of $u_h(\vec{\alpha})$ given by Eqs (35)-(37). □

Corollary. Calculation of the expansion coefficients $\vec{\xi}$, $\{\vec{\dot{\xi}}_\mu\}$, and $\{\vec{\ddot{\xi}}_{\mu\mu'}\}$ are solutions of the following linear system:

$$\mathbf{A}\vec{X} \;=\; \overrightarrow{b} \tag{45}$$

where $\mathbf{A}$ is an $N_\phi \times N_\phi$, Hermitian and positive definite matrix, whose entries are of the form, $a\left(\phi_j^K, \phi_l^{K'}\right)$; $\forall K, K' \in \mathcal{T}_h$, $1 \le j \le n^K$, and $1 \le l \le n^{K'}$, with the bilinear form, $a(\cdot,\cdot)$, defined in Eq. (28). The expression of the vector $\vec{b}$ depends on the target expansion coefficients as follows:

roman*. For $\vec{X} = \vec{\xi}$, the j^{th} coordinate of the vector $\vec{b}$ is given by:

$$b_j = F(\psi_j^K(\alpha^K)) \;; \quad \forall j = 1, \cdots n^K, \; \forall K \in \mathcal{T}_h \tag{46}$$

with the linear functional F given in Eq. (29).

roman*. For $\vec{X} = \vec{\dot{\xi}}_\mu$, the j^{th} coordinate of vector $\vec{b}$ is given by:

$$b_j = G(\psi_j^K(\alpha^K)) \;; \quad \forall j = 1, \cdots n^K, \; \forall K \in \mathcal{T}_h \tag{47}$$

with the linear functional G given in Eq. (41).

roman*. For $\vec{X} = \vec{\ddot{\xi}}_{\mu\mu'}$, the j^{th} coordinate of vector $\vec{b}$ is given by:

$$b_j = G(\psi_j^K(\alpha^K)) \;; \quad \forall j = 1, \cdots n^K, \; \forall K \in \mathcal{T}_h \tag{48}$$

with the linear functional G given in Eq. (42).

□

Upon determination of the set of differentiated expansion coefficients, $\{\dot{\xi}_\mu\}$ and $\{\ddot{\xi}_{\mu\mu'}\}$, by the above procedure, the Hessian, $\ddot{\mathbf{L}}(\vec{\alpha})$ of the Newton system Eq. (23) can be constructed. At the algebraic level, Eq. (23) becomes:

$$\mathbf{M}^{(m)}\vec{X}^{(m)} = \vec{b}^{(m)} \tag{49}$$

where $\mathbf{M}^{(m)}$ is an $N_\Omega \times N_\Omega$ real and symmetric matrix, whose entries are given by $M_{\mu\mu'}(\vec{\alpha}^{\,m}) = \ddot{L}_{\mu\mu'}(\vec{\alpha}^{\,m})$(see Eq. (34)). Matrix $\mathbf{M}$ is dense, but is of much smaller dimension than the least-squares matrix $\mathbf{A}$ since $N_\Omega << N_\phi$. Hence, the linear system given by Eq. (49) can be solved using any direct method.

3.2.3 LSM-WT algorithm: Summary

The proposed solution methodology for tracking the propagation direction of the field with the local basis functions, can be viewed as the following three-step strategy.

Step roman*. **Initialization**
Define $\mathcal{T}_h$, the partition into N_h elements K of the computational domain Ω, see Fig. 4 for illustration, and for each element K, select a set of n^K plane-waves $\left(\phi_j^K\right)_{j=1,\cdots,n^K}$. Note that specifying a constant value for n^K, i.e., stipulating the same number of basis functions for all elements in $\mathcal{T}_h$, is the simplest choice and commonly used. Finally, we select the number and location of the subdomains, e.g., the contiguously colored regions in Fig. 4, where we would be optimizing the angles of the basis functions. In the considered mesh discretization, we chose h to be the element edge length along the radial direction.

Step roman*. **At iteration** m
Evaluate $u_h(\vec{\alpha}^{\,(m)})$ and first- and second-order Fréchet derivatives $\dot{u}_h(\alpha^{(m)})$ and $\ddot{u}_h(\vec{\alpha}^{\,(m)})$ by solving one linear system, $\mathbf{A}\vec{X}$=rhs, (see Eq. (45)), where $\mathbf{A}$ is an $N_\phi \times N_\phi$, Hermitian and positive definite matrix. $\mathbf{A}$ is a sparse matrix with a stencil with of $5n^K$. This task requires evaluation of $\frac{1}{2}(N_\Omega+1)(N_\Omega+2)$ different right-hand sides as defined in Eqs. (46), (47), and (48). Then we determine the update $\delta\vec{\alpha}^{\,(m)}$ by solving the linear system $\mathbf{M}\vec{X}$=$\vec{b}$ (see Eq. (49)), where $\mathbf{M}$ is an $N_\Omega \times N_\Omega$, real, symmetric and dense matrix. The orientational angles of the basis functions are then updated, $\vec{\alpha}^{\,(m+1)}$=$\vec{\alpha}^{(m)}$+$\delta\vec{\alpha}^{\,(m)}$.

Step roman*. **Stopping criterion**
To stop the algorithm, we first record all the angles of basis functions in a $n_h \times n^K$ rectangular array, $\boldsymbol{\alpha}^{(m)}$, and their corresponding updates in a rectangular array $\boldsymbol{\delta\alpha}^{(m)}$. We stop the algorithm when the relative successive variation, $\frac{||\boldsymbol{\delta\alpha}^{(m)}||}{||\boldsymbol{\alpha}^{(m)}||}$, is less than a prescribed tolerance level. The numerical investigation tends indicates that 5% is a practical tolerance level, as illustrated in Sec. 5.

Remark 2. The proposed formulation can also accommodate p-type refinement, in which the number of plane-waves can be apportioned differently from element to element, i.e., n^K need not necessarily be considered constant.

4 Mathematical Analysis

Throughout this section, we adopt the following notations and assumptions:

- $\mathcal{T}_h$ is a *regular* triangulation of the computational domain $\overline{\Omega}$ into triangular- or rectangular-shaped elements K i.e. there exists a positive constant $\hat{c}$ that depends on Ω only such that:

$$\forall\, K \in \mathcal{T}_h \;;\; \frac{h_K}{\rho_K} \leq \hat{c}|K|, \tag{50}$$

  where ρ_K denotes the radius of the disc inscribed in the element K centered at x_G, the gravity center of K [31]. Note that h_e is the length of the edge e of the element K i.e. $h_K = \max_{e\subset\partial K} h_e$ and $h = \max_{K\in\mathcal{T}_h} h_K$.

- For $K \in K \in \mathcal{T}_h$, we define the local space $V(K)$ as follows:

$$V(K) \;=\; \left\{v \in H^1(K);\; \middle|\; \Delta v + k^2 v = 0 \text{ in } K \text{ and } \partial_n v \in L^2(\partial K)\right\}. \tag{51}$$

- V is a global space given by:

$$V \;=\; \left\{v \in L^2(\Omega);\; \middle|\; \forall\, K \in \mathcal{T}_h,\; v_{|_K} \in V(K)\right\}. \tag{52}$$

- For $v \in V$, we denote by $|||\cdot|||$ the norm associated with the hermitian bilinear form $a(\cdot,\cdot)$, given by Eq.(28), as follows:

$$|||v||| \;=\; \{a(v,v)\}^{1/2}, \tag{53}$$

  that is,

$$\begin{aligned} |||v|||^2 = &\sum_{\text{e:interior edge}} \left(\frac{1}{k^2 h_e}\,\|[[\partial_n v]]\|^2_{0,e} + \frac{1}{h_e}\,\|[v]\|^2_{0,e}\right) \\ &+ \sum_{e\subset\Gamma} \frac{1}{k^2 h_e}\,\|\partial_n v\|^2_{0,e} + \sum_{e\subset\Sigma} \frac{1}{k^2 h_e}\,\|\partial_n v - \mathrm{i}kv\|^2_{0,e}. \end{aligned} \tag{54}$$

- For each element $K \in \mathcal{T}_h$, $||\cdot||_{0,K}$ (resp. $|\cdot|_{1,K}$) is the L^2-norm (resp. H^1 semi-nom) on K.

- The following two classical inequalities [31] will be of subsequent use:

$$\|w\|_{0,e} \;\leq\; \hat{c}\left(\frac{1}{h_K^{1/2}}\|w\|_{0,K} + h_K^{1/2}|w|_{1,K}\right), \tag{55}$$

$$\|\partial_n w\|_{0,e} \;\leq\; \hat{c}\left(\frac{1}{h_K^{1/2}}|w|_{1,K} + h_K^{\theta-3/2}|w|_{\theta,K}\right). \tag{56}$$

We recall the following standard properties that will be of subsequent use:

Property 4.1.

roman*. Let $J(\cdot)$ be the cost function given by Eq.(25). Then,

$$J(v) \;=\; \tfrac{1}{2}a(v,v) - \Re(F(v)) + \tfrac{1}{2}\sum_{e\subset\Gamma} \frac{1}{k^2 h_e}\,||g||^2_{L^2(e)} \;;\forall\; v \in V, \tag{57}$$

with $\Re(z)$ representing the real part of $z \in \mathbb{C}$. Observe that:

$$J(v) \;=\; 0 \text{ if and if } \; \mathrm{v} \in H^1(\Omega) \cap V \text{ and } v \text{ satisfies BVP(1)}.$$

roman*. Assume Ω to be a polygonal-shaped domain. Then, for any $g \in H^s(\Gamma)$ with $s > 0$, the solution of BVP(1), $u \in H^\theta(\Omega)$, where $\theta \in (3/2, 2]$. Hence, $u \in V$ and $J(u) = 0$.

4.1 Announcement of the Main Results

The following two theorems summarize the main results of this section. The first result provides an a priori error estimate.

Theorem 4.1. Let u (reps. u_h) be the solution of the boundary value problem BVP(1) (reps. the variational problem VF(27)). Then there exists a positive constant $\hat{c}$ ($\hat{c}$ depends on Ω only) such that:

$$||u - u_h||_{L^2(\Omega)} \leq \hat{c}\,(1 + kh) \inf_{v_h \in V_h} |||u - v_h|||, \tag{58}$$

where V_h is any finite dimensional subspace of the space V given by Eq(52).

The next result provides a posteriori error estimates that depend on the regularity of the scattered field u, the solution of BVP(1).

Theorem 4.2. Let u (reps. u_h) be the solution of the boundary value problem BVP(1) (reps. the variational problem VF(27)). Then, there exists a positive constant $\hat{c}$ ($\hat{c}$ depends on Ω only) such that for $kh << 1$, we have:

$$||u - u_h||_{L^2(\Omega)} \leq \hat{c} \left(\sum_{e \subset \Gamma} \frac{1}{k^2 h_e} \int_e (g - \partial_n u_h)\, \overline{g}\, ds \right)^{1/2}. \tag{59}$$

In addition, if $u \in H^{N+2}(\Omega)$, then there exists a positive constant $\hat{c}$ ($\hat{c}$ depends on Ω and N only) such that for $kh << 1$, we have:

$$||u - u_h||_{L^2(\Omega)} \leq \hat{c}\,(kh)^{N-1} \left(k^s \, \|g\|_{1/2-s,\Gamma} + \sum_{l=0}^{N-1} \frac{1}{k^{l+1}} \, \|g\|_{l+1/2,\Gamma} \right). \tag{60}$$

where $s \in (1/2, 1)$.

Remark 3. The following two observation are noteworthy:

- Theorem 4.2 provides a practical a posteriori error estimate that can be employed for an adaptive mesh refinement and/or subdomain partitioning strategy yielding $\{\Omega_\mu\}$. This estimate is very simple to evaluate at it involves the computation of the normal derivative of the scattered field over the edges of the interior boundary Γ. These quantities do not add to the cost of the calculation, as they have been determined when building the matrix $\mathbf{A}$.
- When the incident field is a plane wave, the expression of g is given by Eq.(2), which is an analytical function. Hence, the regularity of u depends mainly on the regularity of the boundary Γ (since in practice the exterior boundary Σ is an artificial boundary that can be chosen to be regular enough). Moreover, for the case of g given by Eq.(2), we have $\|g\|_{s,\Gamma} \leq 1$ for any $s > 0$. Therefore, since $k \geq 1$, the a posteriori estimate given by Eq.(60) becomes:

  $$||u - u_h||_{L^2(\Omega)} \leq \hat{c}\,(kh)^{N-1}\, k^s, \tag{61}$$

  where $s \in (1/2, 1)$.

4.2 Preliminary Properties and Intermediate Estimates

The goal of this section is to establish the properties and estimates needed to prove Theorem 4.1 and Theorem 4.2.

4.2.1 Preliminary Properties

Let V_h be any finite dimensional subspace of the space V given by Eq.(52). Consider the following variational problem:

$$\text{(VF)} \quad \begin{cases} \text{Find } u_h \in V_h \text{ such that :} \\ a(u_h\ ,\ w) \ = \ F(w)\ ;\ \forall w \in V_h, \end{cases} \tag{62}$$

where $a(\cdot,\cdot)$ (resp. $F(\cdot)$) is the bilinear form reps.(the linear) form given by Eq.(28) (resp. Eq.(29)).

Then, we have the following useful properties pertaining to the bilinear form $a(\cdot,\cdot)$ and the cost function $J(\cdot)$ given by Eq. (25) or Eq.(57):

Property 4.2. Let u (reps. u_h) be the solution of the boundary value problem BVP(1) (resp. the variational problem VF(62). Then, we have:

$$J(u_h) \ = \ \inf_{v_h \in V_h} J(v_h). \tag{63}$$

roman*.

roman*.

$$a(u - u_h, v_h) \ = \ 0\ ; \quad \forall v_h \in V_h. \tag{64}$$

roman*.

$$a(u - u_h, u) \ = \ \sum_{e \subset \Gamma} \frac{1}{k^2 h_e} \int_e (g - \partial_n u_h)\, \overline{g}\ ds. \tag{65}$$

roman*.

$$a(u - u_h, u - v_h) \ = \ a(u - u_h, u)\ ; \quad \forall v_h \in V_h. \tag{66}$$

Proof. Using the property of the cost function $J(\cdot)$ given by Eq.(57) (See Property (4.1)) and the fact that u_h is the solution of the variational problem VF(62), we obtain:

$$J(v_h) - J(u_h) = \frac{1}{2} a(v_h - u_h, v_h - u_h)\ ; \quad \forall v_h \in V_h. \tag{67}$$

Hence, it follows from the definition of the norm $|||\cdot|||$ (See Eq.(54)) that:

$$J(v_h) \ = \ J(u_h) + \frac{1}{2}\, |||v_h - u_h|||^2\ ; \quad \forall v_h \in V_h, \tag{68}$$

which concludes the proof of Property i.
To establish Property ii, we first observe that it follows from VF(27) that:

$$a(u, v_h) \ = \ F(v_h)\ ; \quad \forall v_h \in V_h \subseteq V. \tag{69}$$

Hence, Property ii is a direct consequence of combining Eq.(69) and the fact that u_h satisfies VF(62).
Next, we prove Property iii. To this end, we use the fact that u (resp. u_h) be the solution of the variational problem VF(27) (reps. VF(62)). We then have:

$$a(u - u_h, u) \ = \ F(u) - \overline{F(u_h)}. \tag{70}$$

Hence, using the definition of $F(\cdot)$ (See Eq(29)), we deduce that:

$$a(u - u_h, u) \ = \ \sum_{e \subset \Gamma} \frac{1}{k^2 h_e} \left(\int_e g\, \overline{\partial_n u}\ ds \ - \ \overline{\int_e g \partial_n u_h\ ds} \right). \tag{71}$$

which proves to Property iii.
Property iv results immediately from Property ii.

□

The next results are stability estimates on the solution of the boundary value problem BVP(1).

Lemma 4.1. *Assume Ω to be a polygonal-shaped domain and $k \geq 1$. Let $u \in H^1(\Omega)$ be the solution of BVP(1) with a boundary condition $g \in L^2(\Gamma)$. Then, for any $s \in (1/2, 1]$, there is a positive constant denoted by $\hat{c}$ that depends on Ω and s only such that:*

$$|u|_{1,\Omega} + k \, \|u\|_{0,\Omega} \leq \hat{c} \, k^s \, \|g\|_{\frac{1}{2}-s,\Gamma}. \tag{72}$$

In addition, if Ω is $\mathcal{C}^\infty$ and $g \in H^{N+1/2}(\Gamma)$, for $N \in \mathbb{N}$, then $u \in H^{N+2}(\Omega)$ and there is a positive constant, denoted by $\hat{c}$ that depends on Ω and s only such that for any integer m such that $2 \leq m \leq N+2$, we have:

$$\|u\|_{m,\Omega} \leq \hat{c} \left(k^{m-1+s} \, \|g\|_{\frac{1}{2}-s,\Gamma} + \sum_{l=0}^{m-2} k^{m-1-l} \, \|g\|_{l+1/2,\Gamma} \right). \tag{73}$$

Proof. Let $g \in L^2(\Gamma)$ and consider $w \in H^1(\Omega)$ the unique solution of the following Laplace-problem:

$$\left\{ \begin{array}{rcll} -\Delta w + k^2 w & = & 0 & \text{in } \Omega, \\ \partial_n w & = & g & \text{on } \Gamma, \\ \partial_n w - \mathrm{i}kw & = & 0 & \text{on } \Sigma. \end{array} \right. \tag{74}$$

Next, we set $\varphi = u - w$. Then, $\varphi \in H^1(\Omega)$ and satisfies the following BVP:

$$\left\{ \begin{array}{rcll} \Delta \varphi + k^2 \varphi & = & 2k^2 \, w & \text{in } \Omega, \\ \partial_n \varphi & = & 0 & \text{on } \Gamma, \\ \partial_n \varphi - \mathrm{i}k\varphi & = & 0 & \text{on } \Sigma. \end{array} \right. \tag{75}$$

Therefore, there is a positive constant, denoted by $\hat{c}$, that depends on Ω only such that [32]:

$$k \, \|\varphi\|_{0,\Omega} + |\varphi|_{1,\Omega} + \leq \hat{c} \, k^2 \, \|w\|_{0,\Omega}. \tag{76}$$

In addition, since w is the solution of the Laplace-problem given by (74), then w satisfies:

$$|w|^2_{1,\Omega} + k^2 \, \|w\|^2_{0,\Omega} - \mathrm{i}k \, \|w\|^2_{0,\Sigma} \; = \; \int_\Gamma g \overline{w} \, ds. \tag{77}$$

We then deduce from taking the real part of Eq.(77) and the fact that $k \geq 1$ that:

$$\|w\|^2_{1,\Omega} \leq |w|^2_{1,\Omega} + k^2 \, \|w\|^2_{0,\Omega} \; \leq \; \left| \int_\Gamma g \overline{w} \, ds \right| \; \leq \; \|g\|_{\frac{1}{2}-s,\Gamma} \, \|w\|_{s-\frac{1}{2},\Gamma}, \tag{78}$$

for any $s \in (1/2, 1]$.
On the other hand, there is also a positive constant denoted again by $\hat{c}$ that depends on Ω and s only such that:

$$\|w\|_{s-\frac{1}{2},\Gamma} \; \leq \; \hat{c} \, \|w\|_{s,\Omega} \; \leq \; \hat{c} \, \|w\|^{1-s}_{0,\Omega} \, \|w\|^s_{1,\Omega}. \tag{79}$$

Hence, it follows from Eq.(78) and Eq.(79) that:

$$\|w\|_{s-\frac{1}{2},\Gamma} \; \leq \; \hat{c} \, k^{s-1} \left(k^2 \|w\|^2_{0,\Omega} \right)^{\frac{1-s}{2}} \left(\|w\|^2_{1,\Omega} \right)^{\frac{s}{2}}. \tag{80}$$

Moreover, using Eq.(78), it follows from Eq.(80) that:

$$\|w\|_{s-\frac{1}{2},\Gamma} \;\leq\; \hat{c}\, k^{s-1} \left| \int_\Gamma g\overline{w}\, ds \right|^{1/2} \tag{81}$$

Consequently, it follows from Eq.(78) and Eq.(81) that there is also a positive constant denoted again by $\hat{c}$ that depends on Ω and s only such that:

$$\left| \int_\Gamma g\overline{w}\, ds \right| \;\leq\; \hat{c}\, k^{s-1} \|g\|_{\frac{1}{2}-s,\Gamma} \left| \int_\Gamma g\overline{w}\, ds \right|^{1/2} \tag{82}$$

and thus,

$$\left| \int_\Gamma g\overline{w}\, ds \right|^{1/2} \;\leq\; \hat{c}\, k^{s-1} \|g\|_{\frac{1}{2}-s,\Gamma}. \tag{83}$$

Finally, it follows from Eq.(78) and Eq.(83) that there is also a positive constant denoted again by $\hat{c}$ that depends on Ω and s only such that:

$$|w|_{1,\Omega} + k\, \|w\|_{0,\Omega} \;\leq\; \hat{c}\, k^{s-1} \|g\|_{\frac{1}{2}-s,\Gamma}. \tag{84}$$

Furthermore, since $u = \varphi + w$, it follows from Eq.(76) and Eq.(77) that there is also a positive constant denoted again by $\hat{c}$ that depends on Ω and s only such that:

$$k\, \|u\|_{0,\Omega} + |u|_{1,\Omega} \;\leq\; \hat{c}\, \left(k^2\, \|w\|_{0,\Omega} + |w|_{1,\Omega} + k\, \|w\|_{0,\Omega} \right). \tag{85}$$

Hence, we obtain from Eq.(84) and Eq.(85) that there is also a positive constant denoted again by $\hat{c}$ that depends on Ω only such that:

$$|u|_{1,\Omega} + k\, \|u\|_{0,\Omega} \leq\; \hat{c}\, k^s\, \|g\|_{\frac{1}{2}-s,\Gamma}, \tag{86}$$

which concludes the proof of Eq.(72).
Next, we prove Eq.(73). To this end, assume $g \in H^{N+1/2}(\Gamma)$, for $N \in \mathbb{N}$. We use the induction to prove that $u \in H^{N+2}(\Omega)$. First, we know that $u \in H^1(\Omega)$. For $1 \leq m \leq N+1$, assume $u \in H^m(\Omega)$. Therefore, $u_{|\partial\Omega} \in H^{m-\frac{1}{2}}(\partial\Omega)$ with $\frac{1}{2} \leq m - \frac{1}{2} \leq N + \frac{1}{2}$. Moreover, if follows from the regularity of g, that $\partial_n u_{|\partial\Omega} \in H^{m-\frac{1}{2}}(\partial\Omega)$. On the other hand, $\Delta u \;=\; k^2\, u \in H^m(\Omega)$. Therefore, $u \in H^{m+1}(\Omega)$ and we have [32]:

$$\|u\|_{m+1,\Omega} \leq\; \hat{c}\, \left(\|\Delta u\|_{m-1,\Omega} + \|\partial_n u\|_{m-\frac{1}{2},\Gamma} \right). \tag{87}$$

for some positive constant $\hat{c}$ that depends on Ω only. Hence, $u \in H^{N+2}(\Omega)$. Furthermore, since u satisfies BVP(1), then for $1 \leq m \leq N+1$, we have:

$$\|u\|_{m+1,\Omega} \leq\; \hat{c}\, \left(k^2 \|u\|_{m-1,\Omega} + \|g\|_{m-\frac{1}{2},\Gamma} + k\, \|u\|_{m-\frac{1}{2},\Sigma} \right). \tag{88}$$

Thus,

$$\|u\|_{m+1,\Omega} \leq\; \hat{c}\, \left(k^2 \|u\|_{m-1,\Omega} + \|g\|_{m-\frac{1}{2},\Gamma} + k\, \|u\|_{m,\Omega} \right). \tag{89}$$

Proceeding by recursion, we then obtain, for $2 \leq m \leq N+2$, that :

$$\|u\|_{m,\Omega} \leq \hat{c}\, \left(k^m\, \|u\|_{0,\Omega} + k^{m-1}\, |u|_{1,\Omega} + \sum_{l=0}^{m-2} k^{m-2-l}\, \|g\|_{l+1/2,\Gamma} \right). \tag{90}$$

which can be re-written as follows:

$$\|u\|_{m,\Omega} \leq \hat{c} \left(k^{m-1} \left(k \|u\|_{0,\Omega} + |u|_{1,\Omega} \right) + \sum_{l=0}^{m-2} k^{m-2-l} \|g\|_{l+1/2,\Gamma} \right). \tag{91}$$

Eq.(73) is then a consequence of substituting Eq.(86) in to Eq.(91)

□

Next, let $v \in V$ and consider $w \in H^1(\Omega)$ the unique solution of the following BVP:

$$\begin{cases} -\Delta w - k^2 w &= v & \text{in } \Omega, \\ \partial_n w &= 0 & \text{on } \Gamma, \\ \partial_n w + \mathrm{i}kw &= 0 & \text{on } \Sigma. \end{cases} \tag{92}$$

The next result states a stability estimate on the solution of BVP(92) assuming that the boundary of the domain Ω is only Lipschitz continuous. Note that a similar result has been established in [sinum] assuming the computational domain being a polygonal-shaped domain. Similar estimates with different approaches can be found for example in [25] and references therein.

Lemma 4.2. *Assume Ω to bea polygonal-shaped domain and $k \geq 1$. Then, $w \in H^\theta(\Omega)$, where $\theta \in (3/2, 2]$. In addition, there is a positive constant $\hat{c}$, that depends on Ω and θ only, such that:*

$$k \|w\|_{0,\Omega} + k^{1-\theta} |w|_{\theta,\Omega} \ \leq \ \hat{c} \|v\|_{0,\Omega}. \tag{93}$$

Proof. The regularity of $w \in H^\theta(\Omega)$, with $\theta \in (3/2, 2]$ results from standard regularity results of the Laplace operator [28]and [32]. In addition, we have:

$$\|w\|_{\theta,\Omega} \leq \hat{c} \left\{ \|v + k^2 w\|_{\theta-2,\Omega} + \|k w\|_{\theta-3/2,\Sigma} \right\}. \tag{94}$$

for some positive constant $\hat{c}$, that depends on Ω and θ only.
In addition, since $w \in V$, we have:

$$k \|w\|_{0,\Omega} + |w|_{1,\Omega} \leq \hat{c} \|v\|_{0,\Omega}, \tag{95}$$

Next, we estimate $|w|_{\theta,\Omega}$. To this end, we proceed in two steps.
Step 1. The goal here is to prove that

$$\|w\|_{\theta-3/2,\Sigma} \leq \frac{\hat{c}}{k^{2-\theta}} \|v\|_{0,\Omega}. \tag{96}$$

To this end, we first consider the the following standard estimate:

$$\|w\|_{\theta-3/2,\Sigma} \leq \hat{c} \|w\|_{\theta-1,\Omega}. \tag{97}$$

In addition, since $\dfrac{1}{2} < \theta - 1 < 1$, then we also have the following interpolation result [28]:

$$\|w\|_{\theta-1,\Omega} \leq \|w\|_{0,\Omega}^{2-\theta} \|w\|_{1,\Omega}^{\theta-1}. \tag{98}$$

Therefore, Eq.(97) becomes:

$$\|w\|_{\theta-3/2,\Sigma} \leq \hat{c} \ \|w\|_{0,\Omega}^{2-\theta} \|w\|_{1,\Omega}^{\theta-1} \tag{99}$$

Furthermore, since $k \geq 1$, it follows from (95) that:

$$\|w\|_{1,\Omega} \leq \left(k^2 \|w\|_{0,\Omega}^2 + |w|_{1,\Omega}^2\right)^{1/2} \leq \hat{c}\, \|v\|_{0,\Omega} \tag{100}$$

and

$$\|w\|_{0,\Omega} \leq \frac{\hat{c}}{k} \|v\|_{0,\Omega}. \tag{101}$$

Eq.(96) is then an immediate consequence of Eq.(99), Eq.(100), and Eq.(101).
Step 2. The goal here is to prove that:

$$\|w\|_{\theta-2,\Omega} \leq \frac{\hat{c}}{k^{3-\theta}} \|v\|_{0,\Omega}. \tag{102}$$

It follows from BVP(92) that:

$$k^2 \|w\|_{-1,\Omega} = \|\Delta w + v\|_{-1,\Omega}. \tag{103}$$

Hence,

$$k^2 \|w\|_{-1,\Omega} \leq |w|_{1,\Omega} + \|v\|_{-1,\Omega}. \tag{104}$$

Consequently, there is a positive constant, denoted by $\hat{c}$, that depends on Ω only such that:

$$k^2 \|w\|_{-1,\Omega} \leq |w|_{1,\Omega} + \hat{c}\, \|v\|_{0,\Omega}. \tag{105}$$

Then, it follows from Eq.(95) and Eq.(105) that there is a positive constant, denoted again by $\hat{c}$, that depends on Ω only such that:

$$k^2 \|w\|_{-1,\Omega} \leq \hat{c}\, \|v\|_{0,\Omega}. \tag{106}$$

Furthermore, using again Eq.(95), we deduce from Eq.(106) that there is a positive constant, denoted again by $\hat{c}$, that depends on Ω only such that:

$$k^2 \|w\|_{-1,\Omega} + k \|w\|_{0,\Omega} \leq \hat{c}\, \|v\|_{0,\Omega}. \tag{107}$$

We then conclude the proof of Eq.(102) using standard interpolation results [28] and the fact that $-\frac{1}{2} < \theta - 2 \leq 0$.
We are now ready to prove Eq.(93). First, we have from Eq.(94) that:

$$\|w\|_{\theta,\Omega} \leq \hat{c}\, \left\{ \|v\|_{\theta-2,\Omega} + k^2 \|w\|_{\theta-2,\Omega} + \|k\, w\|_{\theta-3/2,\Sigma} \right\}. \tag{108}$$

Next, it follows from substituting Eq.(96), and Eq.(102) into Eq.(108), that there is a positive constant, denoted again by $\hat{c}$, that depends on Ω only such that:

$$\|w\|_{\theta,\Omega} \leq \hat{c}\, \left\{ \|v\|_{0,\Omega} + k^{\theta-1} \|v\|_{0,\Omega} + k^{\theta-1} \|v\|_{0,\Omega} \right\}. \tag{109}$$

Therefore, Eq.(93) results immediately for using $k \geq 1$ and $\theta \in (3/2, 2]$ into Eq.(109).

□

4.2.2 Interpolation Properties

We adopt throughout this paragraph the following additional notations:

- For $K \in \mathcal{T}_h$, let $\overrightarrow{x}_G$ be the gravity center of K and ρ_K the radius of the circle inscribed in K whose center is $\overrightarrow{x}_G$. Since the triangulation $\mathcal{T}_h$ is regular, then there is a positive constant denoted by $\hat{c}$ that depends on Ω only such that:

$$\frac{h_K}{\rho_K} \leq \hat{c} \tag{110}$$

  where h_K satisfies $h_K = \max_{e \subset \partial K} h_e$.

- We set:

$$r_K = \min\left(\rho_K, \frac{\pi}{3\,k}\right) \tag{111}$$

  and consider $B_K = B(\overrightarrow{x}_G, r_K)$, the ball of radius r_K centered at $\overrightarrow{x}_G$. Hence, $B_K \subseteq K$. In addition, $\forall \overrightarrow{x} \in B_K$ and for any $\overrightarrow{d}$ such that $|\overrightarrow{d}| = 1$, we have:

$$\left| k\overrightarrow{d} \cdot (\overrightarrow{x} - \overrightarrow{x}_G) \right| \leq \frac{\pi}{3} \tag{112}$$

  and

$$\cos\left(k\overrightarrow{d} \cdot (\overrightarrow{x} - \overrightarrow{x}_G)\right) \geq \frac{1}{2}. \tag{113}$$

- Let $M \in \mathbb{N}$, we set the following M plane waves:

$$\phi_q(\overrightarrow{x}) \;=\; e^{\mathrm{i}\, k \overrightarrow{d_q} \cdot (\overrightarrow{x} - \overrightarrow{x}_G)};\; q = 1, 2, \cdots, M \tag{114}$$

  where $\overrightarrow{d_q}$ is a unit vector representing the direction of the propagation of ϕ_q. Note that, using Eq.(112) and Eq.(113), we obtain $\phi_q(\overrightarrow{x})$ satisfies the following property:

$$\frac{1}{|B_K|} \left| \int_{B_K} \phi_q(\overrightarrow{x})\, d\overrightarrow{x} \right| \geq \frac{1}{2};\; q = 1, 2, \cdots, M. \tag{115}$$

- For $q = 1, 2, \cdots, M$, the direction of propagation $\overrightarrow{d_q}$ is written as follows: $\overrightarrow{d_q} = (d_{q_1}, d_{q_2})$. In addition, we set:

$$z_q \;=\; d_{q_1} + \mathrm{i}\, d_{q_2};\; q = 1, 2, \cdots, M. \tag{116}$$

  Hence, $|z_q| = 1$ for $q = 1, 2, \cdots, M$.

- We set $N = 2M + 1$. Then, for $K \in \mathcal{T}_h$, $Z(K)$ is a subspace of $H^N(K)$, given by:

$$Z(K) \;=\; \left\{ v \in H^N(K);\quad \Delta v + k^2 v = 0 \text{ in } K \right\}. \tag{117}$$

- $Z_h(K)$ is a finite-dimensional subspace of $Z(K)$ defined by:

$$Z_h(K) \;=\; \left\{ v : K \to \mathbb{C} \;\middle|\; v \;=\; \sum_{q=1}^{M} \beta_q \phi_q; \quad \text{where } \beta_q \in \mathbb{C} \right\}. \tag{118}$$

The next proposition states preliminary interpolation properties to be employed to establish estimates on the interpolation operator.

Proposition 4.1. *For $K \in \mathcal{T}_h$, there is a linear mapping*

$$\Pi_N : Z(K) \longrightarrow Z_h(K)$$

such that, $\forall v \in Z(K)$, we have:

$$\int_{B_K} \partial^m \left(v - \Pi_N v\right)\, d\overrightarrow{x} = \int_{B_K} \overline{\partial}^m \left(v - \Pi_N v\right)\, d\overrightarrow{x} = 0 \;; m = 0, \cdots, N \tag{119}$$

where $\partial^m = (\partial_{x_1} + \mathrm{i}\,\partial_{x_2})^m$ and $\overline{\partial}^m = (\partial_{x_1} - \mathrm{i}\,\partial_{x_2})^m$.
Moreover, for any $p \in \mathbb{N}$, there is a positive constant $\hat{c}$, that depends on p and Ω only, such that:

$$|\Pi_N v|_{p,K} \;\leq\; \hat{c}\, k^p \left(1 + k h_K\right) \sum_{m=0}^{N} \frac{1}{k^m} \, |v|_{m,K} \;; \quad \forall v \in Z(K). \tag{120}$$

Proof. Let $v \in Z(K)$, and define the vector $\overrightarrow{b} = (b_1, b_2, \cdots, b_N)^t \in \mathbb{C}^M$ as follows:

$$\left\{ \begin{array}{rcll} b_m & = & \dfrac{1}{(\mathrm{i}\,k)^{N+1-m}} \dfrac{1}{|B_K|} \int_{B_K} \overline{\partial}^{N+1-m} v \, d\overrightarrow{x} & m = 1, 2, \cdots, N \\ b_{N+1} & = & \int_{B_K} v \, d\overrightarrow{x} & \\ b_{m+N+1} & = & \dfrac{1}{(\mathrm{i}\,k)^{m}} \dfrac{1}{|B_K|} \int_{B_K} \partial^{m} v \, d\overrightarrow{x} & m = 1, 2, \cdots, N. \end{array} \right. \tag{121}$$

We also consider the matrix $A \in \mathbb{C}^{M,M}$ defined by

$$A_{mq} \;=\; z_q^{m-1} \;, \quad 1 \leq m, q \leq M. \tag{122}$$

Observe that A is invertible and $\|A^{-1}\|_2$ does not depend on K, k, and r_K given by Eq.(111). Hence, there is a unique $\overrightarrow{\xi} \in \mathbb{C}^M$ and a positive constant, denoted by $\hat{c}$, that depends on Ω only such that:

$$A\,\overrightarrow{\xi} \;=\; \overrightarrow{b} \tag{123}$$

and

$$\|\,\overrightarrow{\xi}\,\|_2 \leq \hat{c}\,\|\,\overrightarrow{b}\,\|_2.$$

On the other hand, it follows from Eq.(121) that:

$$\begin{array}{rcl} \|\,\overrightarrow{b}\,\|_2^2 \;=\; \displaystyle\sum_{m=1}^{M} |b_m|^2 = \sum_{m=1}^{N} \frac{1}{k^{2(N+1-m)}} \frac{1}{|B_K|^2} \left| \int_{B_K} \overline{\partial}^{N+1-m} v \, d\overrightarrow{x} \right|^2 & & \\ \quad + \dfrac{1}{|B_K|^2} \left| \displaystyle\int_{B_K} v \, d\overrightarrow{x} \right|^2 + \sum_{m=1}^{N} \frac{1}{k^{2m}} \frac{1}{|B_K|^2} \left| \int_{B_K} \partial^m v \, d\overrightarrow{x} \right|^2, & & \end{array} \tag{124}$$

and then,

$$\|\,\overrightarrow{b}\,\|_2^2 \;= \frac{1}{|B_K|^2} \left| \int_{B_K} v \, d\overrightarrow{x} \right|^2 + \sum_{m=1}^{N} \frac{1}{k^{2m}} \frac{1}{|B_K|^2} \left(\left| \int_{B_K} \overline{\partial}^m v \, d\overrightarrow{x} \right|^2 + \left| \int_{B_K} \partial^m v \, d\overrightarrow{x} \right|^2 \right) \tag{125}$$

Next, for each plane wave ϕ_q given by Eq.(114), z_q given by Eq.(116), and ξ_q given by Eq.(123), we set:

$$\beta_q \;=\; z_q^N \xi_q \, \frac{|B_K|}{\displaystyle\int_{B_K} \phi_q(\overrightarrow{x})\, d\overrightarrow{x}} \;; \quad q = 1, 2, \cdots, M. \tag{126}$$

We also define the interpolation operator Π_N as follows:

$$\Pi_N v \;=\; \sum_{q=1}^{M} \beta_q \, \phi_q \;; \quad \forall v \in Z(K). \tag{127}$$

Since, for each $m \in \mathbb{N}$, we have:

$$\partial^m \phi_q \;=\; (\mathrm{i}\, k)^m \, z_q^m \phi_q \quad \text{and} \quad \overline{\partial}^m \phi_q \;=\; (\mathrm{i}\, k)^m \, \frac{1}{z_q^m} \phi_q,$$

then, it follows from Eq.(127) that:

$$\partial^m \Pi_N v \;=\; \sum_{q=1}^{M} z_q^N \xi_q \, \frac{|B_K|}{\displaystyle\int_{B_K} \phi_q(\overrightarrow{x})\, d\overrightarrow{x}} \, (\mathrm{i}\, k)^m \, z_q^m \phi_q \;; \quad \forall v \in Z(K). \tag{128}$$

Therefore,

$$\int_{B_K} \partial^m \Pi_N v \, d\overrightarrow{x} \;=\; |B_K| \sum_{q=1}^{M} z_q^{N+m} \xi_q \, (\mathrm{i}\, k)^m \;; \quad \forall v \in Z(K). \tag{129}$$

Consequently, using Eq.(122) and Eq.(123), along with the definition of the vector $\overrightarrow{b}$ given by Eq.(121), it follows from Eq.(129) that:

$$\int_{B_K} \partial^m \Pi_N v \, d\overrightarrow{x} \;=\; |B_K| \, (\mathrm{i}\, k)^m \, b_{N+m+1} \;=\; \int_{B_K} \partial^m v \, d\overrightarrow{x} \;; \quad \forall v \in Z(K). \tag{130}$$

Similarly, we also have:

$$\int_{B_K} \overline{\partial}^m \Pi_N v \, d\overrightarrow{x} \;=\; |B_K| \, (\mathrm{i}\, k)^m \, b_{N-m+1} \;=\; \int_{B_K} \overline{\partial}^m v \, d\overrightarrow{x} \;; \quad \forall v \in Z(K). \tag{131}$$

Eq.(130) and Eq.(131) conclude the proof of Eq.(119).
On the other hand, for $p \in \mathbb{N}$ and $K \in \mathcal{T}_h$, it follows from the definition of Π_N given by Eq.(127) that:

$$|\Pi_N v|_{p,K} \;\leq\; \sum_{q=1}^{M} |\beta_q| \, |\phi_q|_{p,K} \;; \quad \forall v \in Z(K). \tag{132}$$

Moreover, using Eq.(126) along with Eq.(115), we deduce that:

$$|\beta_q| \;\leq\; 2\, |\xi_q| \;; q = 1, 2, \cdots, M. \tag{133}$$

Hence,

$$\|\beta\|_2 \;\leq\; 2\, \|\xi\|_2 \;\leq\; 2\, \|A^{-1}\|_2 \, \|b\|_2. \tag{134}$$

In addition, it is easy to verify that for any $K \in \mathcal{T}_h$ and any plane waves ϕ_q given by Eq.(114), there is a positive constant $\hat{c}$ ($\hat{c}$ depends on Ω only) such that:

$$|\phi_q|_{p,K} \;\leq\; \hat{c}\, k^p \, h_K \;; q = 1, 2, \cdots, M. \tag{135}$$

Therefore, it follows from substituting Eq.(134) and Eq.(135) into Eq.(132) that there is a positive constant $\hat{c}$ ($\hat{c}$ depends on Ω only) such that:

$$|\Pi_N v|_{p,K} \;\leq\; \hat{c}\, k^p\, h_K\, \|b\|_2 \;; \quad \forall v \in Z(K). \tag{136}$$

Next, we estimate $\|b\|_2$. To this end, we observe that, by construction, we have:

$$\|b\|_2 \;\leq\; \hat{c} \sum_{m=0}^{N} \frac{1}{|B_K|} \left(\left| \int_{B_K} \partial^m v \; d\overrightarrow{x} \right| + \left| \int_{B_K} \overline{\partial}^m v \; d\overrightarrow{x} \right| \right) \;; \quad \forall v \in Z(K). \tag{137}$$

Hence,

$$\|b\|_2 \;\leq\; \hat{c} \sum_{m=0}^{N} \frac{1}{|B_K|^{1/2}} \left(\|\partial^m v\|_{0,K} + \|\overline{\partial}^m v\|_{0,K} \right) \;; \quad \forall v \in Z(K), \tag{138}$$

and therefore:

$$\|b\|_2 \;\leq\; \frac{\hat{c}}{r_K} \sum_{m=0}^{N} |v|_{m,K} \;; \quad \forall v \in Z(K), \tag{139}$$

where r_K is given by Eq.(111).
Furthermore, it follows from Eqs.(110)-(111) that:

$$\frac{h_K}{r_K} \;\leq\; \max(\hat{c}, \frac{3}{\pi} k h_K) \;\leq\; \hat{c}\,(1 + k h_K) \tag{140}$$

for some positive constant denoted again by $\hat{c}$. Eq.(120) is then an immediate consequence of substituting Eq.(139) and Eq.(140) into Eq.(136). □

Before stating the second interpolation estimate, we prove the following technical Lemma.

Lemma 4.3. *For $K \in \mathcal{T}_h$, consider the subspace*

$$W(K) = \left\{ w \in H^1(K) \;\middle|\; \int_{B_K} w \; d\overrightarrow{x} \;=\; 0 \right\}.$$

Then, there is a positive constant $\hat{c}$ ($\hat{c}$ does not depend on K) such that:

$$\|w\|_{0,K} \;\leq\; \hat{c}\, h_K\, (1 + k h_K)\, |w|_{1,K} \;; \quad \forall w \in W(K). \tag{141}$$

Proof. Indeed, let $\alpha \in \mathbb{C}$. Then, for any $w \in W(K)$, we have:

$$\|w\|_{0,K} \;\leq\; \|w - \alpha\|_{0,K} + |\alpha|\, |K|^{1/2} \;=\; \|w - \alpha\|_{0,K} + \frac{|K|^{1/2}}{|B_K|} \left| \int_{B_K} (w - \alpha) \; d\overrightarrow{x} \right|. \tag{142}$$

Hence, using Eq.(115) and Eq.(140), we deduce that there is a positive constant $\hat{c}$, that depends on Ω only, such that:

$$\|w\|_{0,K} \;\leq\; \|w - \alpha\|_{0,K} + \hat{c}\, \frac{h_K}{r_K} \|w - \alpha\|_{0,B_K} \;\leq\; \hat{c}\,(1 + k h_K)\, \|w - \alpha\|_{0,K}. \tag{143}$$

Finally, we have

$$\inf_{\alpha \in \mathbb{C}} \|w - \alpha\|_{0,K} \;\leq\; \hat{c}\, h_K |w|_{1,K}, \tag{144}$$

which concludes the proof of Lemma 4.3. □

Proposition 4.2. *There is a positive constant $\hat{c}$ such that for any $K \in \mathcal{T}_h$, $v \in Z(K) \cap H^{N+1}(K)$, and $m = 0, 1, \cdots, N$, we have:*

$$|v - \Pi_N v|_{m,K} \;\leq\; \hat{c}\,(1 + kh_K)^{N+1-m}\, h_K^{N+1-m}\, |v - \Pi_N v|_{N+1,K}. \tag{145}$$

Proof. Let $v \in Z(K) \cap H^{N+1}(K)$. Then, $\Pi_N v \in Z_h(K) \subseteq Z(K) \cap H^{N+1}(K)$. Consequently, $w = v - \Pi_N v \in Z(K)$ and therefore, it follows from Eq.(119) (See Proposition (4.1)) that:

$$\int_{B_K} \partial^m w \; d\overrightarrow{x} = \int_{B_K} \overline{\partial}^m w \; d\overrightarrow{x} = 0 \; ; m = 0, \cdots, N. \tag{146}$$

On the other hand, we have

$$\partial_x = \frac{1}{2}\left(\partial + \overline{\partial}\right),$$

$$\partial_y = \frac{1}{2\mathrm{i}}\left(\partial - \overline{\partial}\right),$$

and

$$\Delta = \partial\overline{\partial} = \overline{\partial}\partial.$$

Hence, for $j, l \in \mathbb{N}$ such that $j + l \leq N$, we have:

$$\partial_x^j = \frac{1}{2^j} \sum_{p=0}^{j} \frac{j!}{p!(j-p)!} \partial^p\, \overline{\partial}^{j-p}$$

and

$$\partial_y^l = \frac{1}{(2\mathrm{i})^l} \sum_{q=0}^{l} \frac{l!}{q!(l-q)!} \partial^q\, \overline{\partial}^{l-q}.$$

Consequently, we have

$$\partial_x^j\, \partial_y^l\, w \;=\; \frac{1}{2^{j+l}\,\mathrm{i}^l} \sum_{p=0}^{j} \sum_{q=0}^{l} \frac{j!\,l!}{p!(j-p)!\,q!(l-q)!}\, \partial^{p+q}\, \overline{\partial}^{j+l-p-q}\, w.$$

Observe that if $2(p+q) \leq j+l$, we have $\partial^{p+q}\, \overline{\partial}^{j+l-p-q}\, w = \Delta^{p+q}\, \overline{\partial}^{j+l-2(p+q)}\, w$. In addition, we also have $\Delta^{p+q}\, w = (-k^2)^{p+q}\, w$. Consequently, we have:

$$\partial^{p+q}\, \overline{\partial}^{j+l-p-q}\, w = (-k^2)^{p+q}\, \overline{\partial}^{j+l-2(p+q)}\, w.$$

Since $0 \leq j + l - 2(p+q) \leq j + l \leq N$, then it follows from Eq.(146) that:

$$\int_{B_K} \partial^{p+q}\, \overline{\partial}^{j+l-p-q}\, w \; d\overrightarrow{x} = 0.$$

Furthermore, if $2(p+q) \geq j+l$, we have:

$$\partial^{p+q}\, \overline{\partial}^{j+l-p-q}\, w = \Delta^{j+l-(p+q)}\, \partial^{2(p+q)-(j+l)}\, w = (-k^2)^{p+q}\, \partial^{j+l-2(p+q)}\, w.$$

Similarly, since $0 \leq 2(p+q) - (j+l) \leq 2(J+l) - (j+l) \leq N$, it also follows from Eq.(146) that:

$$\int_{B_K} \partial^{p+q}\, \overline{\partial}^{j+l-p+q}\, w \; d\overrightarrow{x} = 0.$$

Finally, we can conclude, that for any $j, l \in \mathbb{N}$ such that $j + l \leq N$, we have:

$$\int_{B_K} \partial_x^j \, \partial_y^l \, w \, d\overrightarrow{x} = 0.$$

Let $0 \leq m \leq N$ and $j, l \in \mathbb{N}$ such that $j + l = m$. Then, using Lemma 4.3, there is a positive constant $\hat{c}$ ($\hat{c}$ does not depend on K) such that:

$$\|\partial_x^j \, \partial_y^l \, w\|_{0,K} \;\leq\; \hat{c}\,(1 + kh_K)\, h_K \, |\partial_x^j \, \partial_y^l \, w|_{1,K}. \tag{147}$$

Since $j + l = m$, we deduce that:

$$|w|_{m,K} \;\leq\; \hat{c}\,(1 + kh_K)\, h_K \, |w|_{m+1,K} \;; \quad 0 \leq m \leq N. \tag{148}$$

Therefore, there is a positive constant, denoted again by $\hat{c}$ ($\hat{c}$ does not depend on K) such that:

$$|w|_{m,K} \;\leq\; \hat{c}\,(1 + kh_K)^{N+1-m}\, h_K^{N+1-m} \, |w|_{N+1,K} \;; \quad 0 \leq m \leq N. \tag{149}$$

□

The next result is a key estimate for proving the main results of this paper (See Theorem 4.1 and 4.2).

Theorem 4.3. There is a positive constant $\hat{c}$ such that for any $K \in \mathcal{T}_h$, $v \in Z(K) \cap H^{N+1}(K)$, and $m = 0, 1, \cdots, N+1$, we have:

$$|v - \Pi_N v|_{m,K} \;\leq\; \hat{c}\,(1 + kh_K)^{N+2-m}\, h_K^{N+1-m} \; \left(k\,|v|_{N,K} + |v|_{N+1,K}\right). \tag{150}$$

Proof. Let v in $Z(K) \cap H^{N+1}(K)$ and $q = 0, 1, \cdots, N-1$. Then, we have:

$$|v|_{q,K} \;=\; \frac{1}{k^2}\,\|\Delta v\|_{q,K} \;\leq\; \frac{\hat{c}}{k^2}\,|v|_{q+2,K}. \tag{151}$$

Hence,

$$|v|_{q,K} \;\leq\; \frac{\hat{c}}{k^{2p}}\,|v|_{q+2p,K} \;; \quad \text{with } 0 \leq p \leq \frac{N+1-q}{2}. \tag{152}$$

Therefore, we deduce that:

$$|v|_{q,K} \;\leq\; \begin{cases} \dfrac{\hat{c}}{k^{N+1-q}}\,|v|_{N+1,K} & \text{for} \quad N+1-q \;\; \text{even} \\[2ex] \dfrac{\hat{c}}{k^{N-q}}\,|v|_{N,K} & \text{for} \quad N+1-q \;\; \text{odd.} \end{cases} \tag{153}$$

Consequently, it follows from Eq.(153) that there is a positive constant $\hat{c}$ ($\hat{c}$ depends on Ω only) such that:

$$\sum_{q=0}^{N} \frac{1}{k^q}\,|v|_{q,K} \;\leq\; \hat{c}\left(\frac{1}{k^N}\,|v|_{N+1,K} + \frac{1}{k^{N+1}}\,|v|_{N+1,K}\right). \tag{154}$$

Let $m = 0, 1, \cdots, N$ and v in $Z(K) \cap H^{N+1}(K)$. Then, it follows from Eq. (145) (See Proposition 4.2), Eq. (120) (See Proposition 4.1), and Eq.(154) that there is a positive constant, denoted again by $\hat{c}$, that depends on Ω only) such that:

$$|v - \Pi_N v|_{m,K} \;\leq\; \hat{c}\,(1 + kh_K)^{N+1-m}\, h_K^{N+1-m} \; \left(|v|_{N,K} + |\Pi_N v|_{N+1,K}\right). \tag{155}$$

Hence, using Eq.(120), we deduce that:

$$\begin{aligned} |v - \Pi_N v|_{m,K} \;&\leq\; \hat{c}\,(1+kh_K)^{N+1-m}\,h_K^{N+1-m}\;(|v|_{N+1,K}+ \\ &\qquad (1+kh_K)\sum_{q=0}^{N}\frac{k^{N+1}}{k^q}\,|v|_{q,K}) \\ &\leq \hat{c}\,(1+kh_K)^{N+2-m}\,h_K^{N+1-m}\;(k\,|v|_{N,K}+|v|_{N+1,K})\,. \end{aligned} \tag{156}$$

□

A direct application of the previous theorem is the following interpolation error estimate.

Corollary 4.1. *Suppose* $(1+kh_K)\,h_K \leq 1$. *Then, there is a positive constant* $\hat{c}$ *such that for any* $K \in \mathcal{T}_h$, $v \in Z(K) \cap H^{N+1}(K)$, *we have:*

$$|v - \Pi_N v|_{\theta,K} \;\leq\; \hat{c}\,(1+kh_K)^{N+1-\theta}\,h_K^{N+2-\theta}\;(k\,|v|_{N,K}+|v|_{N+1,K})\,, \tag{157}$$

where $3/2 < \theta < 2$.

4.2.3 Intermediate Estimates

We first establish a general result that can be viewed as a stability estimate with respect to $|||\cdot|||$.

Proposition 4.3. *Assume that* Ω *to be a polygonal-shaped domain. Then, there is a positive constant* $\hat{c}$ *(*$\hat{c}$ *depends on* Ω *only) such that:*

$$||v||_{0,\Omega} \leq \hat{c}\,(1+kh)\,|||v||| \;; \quad \forall v \in V \tag{158}$$

Proof. For $v \in V$, consider $w \in H^1(\Omega)$ the unique solution of BVP(92). Note that it follows from the standard regularity results of the Laplace operator [28], [32] that $w \in H^\theta(\Omega)$ with $\theta \in]3/2, 2]$. Next, we multiply the first equation of BVP(92) by $\overline{v}$ and integrate over Ω. Hence, it follows from using Green-Riemann theorem and the fact that v satisfies Helmholtz equation that:

$$\|v\|_{0,\Omega}^2 = \sum_{K\in\mathcal{T}_h}\int_{\partial K}(w\,\partial_n\overline{v} - \overline{v}\partial_n w)\,ds, \tag{159}$$

which can be written as follows:

$$\begin{aligned} \|v\|_{0,\Omega}^2 = &\sum_{\text{e:interior edge}}\int_e (w\,[[\partial_n\overline{v}]] \,-\, [\overline{v}]\,\partial_n w\,)\,ds \\ &+\sum_{e\subset\Gamma}\int_e (w\,\partial_n\overline{v} \,-\, \overline{v}\,\partial_n w\,)\,ds + \sum_{e\subset\Sigma}\int_e (w\,\partial_n\overline{v} \,-\, \overline{v}\,\partial_n w\,)\,ds. \end{aligned} \tag{160}$$

We substitute the boundary conditions of BVP(92) into Eq.(160). We then obtain:

$$\begin{aligned} \|v\|_{0,\Omega}^2 = &\sum_{\text{e:interior edge}}\int_e (w\,[[\partial_n\overline{v}]] \,-\, [\overline{v}]\,\partial_n w\,)\,ds \\ &+\sum_{e\subset\Gamma}\int_e w\,\partial_n\overline{v}\,ds + \sum_{e\subset\Sigma}\int_e w\;(\partial_n\overline{v} \,+\, \mathrm{i}k\,\overline{v}\,)\,ds. \end{aligned} \tag{161}$$

Thus,

$$\begin{aligned}\|v\|^2_{0,\Omega} = &\sum_{\text{e:interior edge}} \int_e \left(w\,[[\partial_n \overline{v}]] \;-\; [\overline{v}]\,\partial_n w\,\right) ds \\ &+ \sum_{e\subset\Gamma} \int_e w\,\partial_n \overline{v}\, ds + \sum_{e\subset\Sigma} \int_e w\,\left(\overline{\partial_n v - \mathrm{i}k\, v}\right) ds.\end{aligned} \tag{162}$$

Next, we apply Cauchy-Schwartz inequality to Eq. (162). We then obtain:

$$\begin{aligned}\|v\|^2_{0,\Omega} \leq &\sum_{\text{e:interior edge}} \left(\|w\|_{0,e}\|\,[[\partial_n v]]\|_{0,e} \;+ \|[v]\|_{0,e}\,\|\partial_n w\|_{0,e}\,\right) \\ &+ \sum_{e\subset\Gamma} \|w\|_{0,e}\,\|\partial_n v\|_{0,e} + \sum_{e\subset\Sigma} \|w\|_{0,e}\,\|\partial_n v - \mathrm{i}kv\|_{0,e}.\end{aligned} \tag{163}$$

Hence, using the definition of $|||\cdot|||$ (See Eq.(54)), we deduce that:

$$\begin{aligned}\|v\|^2_{0,\Omega} \leq &\left\{ \sum_{\text{e:interior edge}} \left(kh_e^{1/2}\|w\|_{0,e} \;+ h_e^{1/2}\|\partial_n w\|_{0,e}\right)\right. \\ &\left. + \sum_{e\subset\partial\Omega} kh_e^{1/2}\,\|w\|_{0,e}\right\} |||v|||.\end{aligned} \tag{164}$$

Consequently, we have:

$$\|v\|^2_{0,\Omega} \leq |||v||| \sum_{K\in\mathcal{T}_h} \sum_{e\subset\partial K} \left(kh_K^{1/2}\|w\|_{0,e} \;+ h_K^{1/2}\|\partial_n w\|_{0,e}\right). \tag{165}$$

Next, we substitute the two classical inequalities given by Eq.(55) and Eq.(56) into Eq. (165). We then obtain:

$$\|v\|^2_{0,\Omega} \leq \hat{c}\,|||v||| \sum_{K\in\mathcal{T}_h} \left(k\|w\|_{0,K} \;+ kh_K|w|_{1,K} + |w|_{1,K} + h_K^{\theta-1}|w|_{\theta,K}\,\right). \tag{166}$$

Therefore, we have:

$$\|v\|^2_{0,\Omega} \leq \hat{c}\,|||v|||\,\left(k\|w\|_{0,\Omega} \;+ (1+kh)|w|_{1,\Omega} + h^{\theta-1}|w|_{\theta,\Omega}\,\right). \tag{167}$$

To conclude the proof we use the stability estimates of Lemma 4.2. It follows from Eq.(167) and Eq.(93) that:

$$\|v\|^2_{0,\Omega} \leq \hat{c}\,|||v|||\,\left(1 + kh + (kh)^{\theta-1}\right)\|v\|_{0,\Omega}. \tag{168}$$

Since $3/2 < \theta \leq 2$, then $1/2 < \theta - 1 \leq 1$. Consequently, it follows from Eq.(168) that there is a positive constant, denoted again by $\hat{C}$ which depends on Ω only, such that:

$$\|v\|_{0,\Omega} \leq \hat{c}\;(1+kh)\;|||v|||.$$

□

In the following, we establish intermediate estimates involving the norm $|||\cdot|||$.

Proposition 4.4. *For $\theta \in (3/2, 2]$, we consider the space:*

$$W_\theta = \left\{ v \in H^\theta(\Omega) \; ; \quad \forall K \in \mathcal{T}_h : v_{|_K} \in V(K) \right\}. \tag{169}$$

where $V(K)$ is the subspace given by Eq.(51).
Then, there exists a positive constant $\hat{c}$, which depends on Ω only, such that for any $v \in W_\theta$, we have:

$$|||v||| \leq \hat{c} \left\{ \sum_{K \in \mathcal{T}_h} \left(\frac{1}{h_K^2} \|v\|_{0,K}^2 + \frac{(1+kh_K)^2}{k^2 h_K^2} |v|_{1,K}^2 + \frac{1}{k^2 h_K^{4-2\theta}} |v|_{\theta,K}^2 \right) \right\}^{1/2}. \tag{170}$$

Proof. Since the considered triangulation $\mathcal{T}_h$ is regular satisfying Eq.(50) and Eq.(110), then it follows from Eq.(54), that there is a positive constant $\hat{c}$, which depends on Ω only, such that for any $v \in W_\theta$, we have:

$$|||v|||^2 \; \leq \; \hat{c} \sum_{K \in \mathcal{T}_h} \sum_{e \subset \partial K} \left(\frac{1}{k^2 h_K} \|\partial_n v\|_{0,e}^2 + \frac{1}{h_K} \|v\|_{0,e}^2 \right). \tag{171}$$

Using the classical inequalities given by Eq.(55) and Eq.(56), it follows from Eq.(171) that there exists a positive constant, denoted again by $\hat{c}$, such that:

$$|||v|||^2 \leq \hat{c} \sum_{K \in \mathcal{T}_h} \left(\frac{1}{k^2 h_K^2} |v|_{1,K}^2 + \frac{1}{k^2 h_K^{4-2\theta}} |v|_{\theta,K}^2 + \frac{1}{h_K^2} \|v\|_{0,K}^2 + |v|_{1,K}^2 \right), \tag{172}$$

which concludes the proof of Proposition 4.2. □

The next result is a general error interpolation estimate with respect of the norm $|||\cdot|||$.

Proposition 4.5. *There is a positive constant $\hat{c}$, that depends on Ω only, such that for $kh << 1$, we have:*

$$|||v - \Pi_N v||| \leq \hat{c}\, h^{N-1} \left(|v|_{N,\Omega} + \frac{1}{k} |v|_{N+1,\Omega} \right) \; ; \forall v \in X \tag{173}$$

where $X = \left\{ v \in H^{N+2}(\Omega) \mid \Delta v + k^2 v = 0 \text{ in } \Omega \right\}$ and the mapping Π_N is defined in Proposition (4.1) (See Eq.(127)).

Proof. To establish Eq.(173), we first use the expression of $|||\cdot|||$ given by Eq.(54).

$$\begin{aligned} |||v - \Pi_N v||| \leq \hat{c} \Bigg(& \sum_{K \in \mathcal{T}_h} \left(\frac{1+kh_K}{kh_K} \right)^2 |v - \Pi_N v|_{1,K}^2 + \frac{1}{(kh_K^{2-\theta})^2} |v - \Pi_N v|_{\theta,K}^2 \\ & + \frac{1}{h_K^2} \|v - \Pi_N v\|_{0,K}^2 \Bigg)^{1/2}. \end{aligned} \tag{174}$$

Then we apply Eq.(150) (SeeTheorem 4.3) in conjunction with Eq.(157), we obtain:

$$\begin{aligned} |||v - \Pi_N v||| \leq \hat{c} \Bigg\{ \sum_{K \in \mathcal{T}_h} & \left[\frac{(1+kh_K)^{2N+4}}{(kh_K)^2} h_K^{2N} + \frac{(1+kh_K)^{2N+4-2\theta}}{(kh_K^{2-\theta})^2} h_K^{2(N+1-\theta)} \right. \\ & \left. + (1+kh_K)^{2N+4} h_K^{2N} \right] \left(k^2 |v|_{N,K}^2 + |v|_{N+1,K}^2 \right) \Bigg\}^{1/2}. \end{aligned} \tag{175}$$

Therefore,

$$|||v-\Pi_N v||| \leq \hat{c}\left(\frac{(1+kh)^{N+2}}{k}\,h^{N-1}+\frac{(1+kh)^{N+2-\theta}}{k}\,h^{N-1}+(1+kh)^{N+2}\,h^N\right) \\ (k\,|v|_{N,\Omega}+|v|_{N+1,\Omega})\,, \tag{176}$$

Therefore, Eq.(173) is an immediate consequence of taking $kh << 1$ in Eq.(176). □

Corollary 4.2. *Assume $\partial\Omega$ to be infinitely differentiable, and let $g \in H^{N+1/2}(\Gamma)$, where $N \in \mathbb{N}$. Then, there is a positive constant $\hat{c}$, that depends on Ω only, such that for $kh << 1$, we have:*

$$|||u-\Pi_N u||| \leq \hat{c}\,(kh)^{N-1}\left(k^s\,\|g\|_{1/2-s,\Gamma}+\sum_{l=0}^{N-1}\frac{1}{k^{l+1}}\,\|g\|_{l+1/2,\Gamma}\right), \tag{177}$$

where u is the solution of $BVP(1)$ and $s \in (1/2,1)$.

Proof. This is a direct consequence of applying Lemma 4.1 (See Eq. (72) - (73)) in conjunction with Eq.(176). Indeed, we have:

$$|||u-\Pi_N u||| \leq \hat{c}\,h^{N-1}\left\{k^{N-1+s}\,\|g\|_{1/2-s,\Gamma}+\sum_{l=0}^{N-2}k^{N-2-l}\,\|g\|_{l+1/2,\Gamma}\right. \\ \left.+\frac{1}{k}\left(k^{N+s}\,\|g\|_{1/2-s,\Gamma}+\sum_{l=0}^{N-1}k^{N-1-l}\,\|g\|_{l+1/2,\Gamma}\right)\right\}. \tag{178}$$

Hence,

$$|||u-\Pi_N u||| \leq \hat{c}\,(kh)^{N-1}\left(k^s\,\|g\|_{1/2-s,\Gamma}+\sum_{l=0}^{N-1}\frac{1}{k^{l+1}}\,\|g\|_{l+1/2,\Gamma}\right). \tag{179}$$

□

4.3 Proof of the Main Results

First, we apply property iv (See Eq.(66) in Property 4.2) with $v_h = u_h$. This leads to:

$$|||u-u_h|||^2 = a(u-u_h,u) = a(u-u_h,u-v_h)\ ;\forall v_h \in V_h. \tag{180}$$

Consequently,

$$|||u-u_h||| = \inf_{v_h\in V_h}|||u-v_h|||. \tag{181}$$

Then, using Eq.(158) (See Proposition (158)), there exists a positive constant $\hat{c}$ that depends on Ω only such that:

$$||u-u_h||_{0,\Omega} \leq \hat{c}\,(1+kh)\inf_{v_h\in V_h}|||u-v_h|||, \tag{182}$$

which concludes the proof of Theorem 4.1. Furthermore, it follows from substituting Eq.(65) (See property iii. in Property 4.2) into Eq.(180) that:

$$|||u-u_h|||^2 = \sum_{e\subset\Gamma}\frac{1}{k^2 h_e}\int_e (g-\partial_n u_h)\,\overline{g}\,ds. \tag{183}$$

Consequently, it follows from Eq.(158) (See Proposition (158)) and Eq.(183) that there exists a positive constant $\hat{c}$ that depends on Ω only such that:

$$||u-u_h||_{0,\Omega} \leq \hat{c}\,(1+kh)\,\left\{\sum_{e\subset\Gamma}\frac{1}{k^2h_e}\int_e (g-\partial_n u_h)\,\overline{g}\,ds\right\}^{1/2}. \tag{184}$$

Taking $kh << 1$ into Eq.(184) concludes the proof of the a posteriori estimate given by Eq.(59) inTheorem 4.2. Similarly, the a posteriori error estimate given by Eq.(60) inTheorem 4.2 results from Proposition 4.3 and Corollary 4.2.

5 Illustrative Numerical Results

We consider a prototypical system comprised of a sound-hard, disk-shaped scatterer of radius $a=1$, embedded in circular domain of radius $R=2$, in the presence of an incident plane-wave impinging from the left, i.e., $\vec{d}$=(1,0). The analytical solution for this configuration is expressed as Fourier series [3, 6].

$$u(r,\theta) = 2\sum_{m=0}^{\infty}{}' (-\mathrm{i})^m \left(C_m^2 \mathrm{H}_m^1(kr) + C_m^1 \mathrm{H}_m^2(kr)\right)\cos(m\theta); \quad a\leq r\leq R, \quad \theta\in[0,2\pi), \tag{185}$$

where the prime on the sum indicates that the first term is halved and the Fourier coefficients C_m^l satisfy:

$$C_m^l = (-1)^l\,\frac{\mathrm{J}_m^{'}(ka)}{\Delta_m}\left(\mathrm{H}_m^{l^{'}}(kR) - \mathrm{i}\,\mathrm{H}_m^l(kR)\right); \quad l=1,2, \tag{186}$$

and

$$\Delta_m \;=\; \mathrm{H}_m^{1^{'}}(ka)\left(\mathrm{H}_m^{2^{'}}(kR) - \mathrm{i}\,\mathrm{H}_m^2(kR)\right) - \mathrm{H}_m^{2^{'}}(ka)\left(\mathrm{H}_m^{1^{'}}(kR) - \mathrm{i}\,\mathrm{H}_m^1(kR)\right). \tag{187}$$

The total relative error of the numerical approximation of the scattered field, u_h, can subsequently be expressed by the modified H^1-norm:

$$||u_h-u||_{\widehat{H^1}(\Omega)} = \left(\sum_K ||u_h-u||^2_{H^1(K)} + \sum_{\partial K\in\mathcal{T}_h} ||u_h^{K'}-u_h^K||^2_{L^2(\partial K\cap\partial K')}\right)^{\frac{1}{2}}. \tag{188}$$

This norm is considered a more accurate indicator than solely the standard, local, H^1-norm as it also takes into account the jump of the solution across the edges of the elements. In this study, the series of the analytical solution, given by Eq. (185) was truncated by selecting the first $2*ka+4$ terms. Previously, we observed that this choice was sufficient to achieve the combined convergence of the sum [3, 24, 9].

Remark 4. In spite of its apparent simplicity, there exists at least three attributes of this disk-shaped scattering mathematical model. Firstly, we can assess the accuracy of the proposed method by evaluating the relative error with respect to the analytical solution, given by Eq. (185). Secondly, the considered configuration admits incoming traveling waves due to reflections at the outer boundary. Thus, the local main direction of field propagation is not readily apparent. This makes the determination of the main local directions of propagation, particularly for the far field, more challenging for the proposed wave-tracking approach, as compared to the situation

where a more efficient absorbing boundary condition is employed. Lastly, for realistic scatterers, e.g., non-convex shaped scatterers, multiple reflections at the scatter's boundary may impede facile determination of the main direction for the near field propagation. The considered configuration includes to some extent such a complication through traveling waves reflected at the exterior boundary. These waves propagate toward the inner boundary and therefore mimic the complexity of the propagation. Hence, the proposed configuration appears to provides an adequate platform for assessing the performance of the proposed wave tracking solution methodology.

The computational domain, Ω, is uniformly discretized into quadrilateral elements by approximating the inner and outer boundary as regular matching polygons and radially partitioning the resultant annulus. The mesh is generated as follows: the number of elements in the angular direction are a factor of 4 the number of radial elements, n_r. The total number of elements in the mesh can thus be calculated as $4n_r^2$, as illustrated in Fig. 4 for the case of $n_r = 4$. To locally approximate the scattered field, each element, contained a basis set of 4 plane-wave functions, centered at the element centroid. The initial angle of the plane-wave basis functions were defined by aligning one function along horizontal axis (1,0) and equally spanning the remaining basis functions by angles in increments of $\pi/2$, (see Eq. (7) with n^K=4).
A systematic approach was employed to assign radially aligned elements within a quadrant to comprise an individual subdomains, in the manner of Fig. 4. As such, the orientation of the elemental basis sets within a given subdomain were locked to a common value. Each subdomain was then replicated to all four quadrants. We recognize that is is not an optimal domain partition, given the propagation of the scattered field is not periodic with respect to the quadrant, nor is it necessarily constant within a given radial cone. Clearly, this partitioning strategy is relatively arbitrary, and definitely not optimal, which may hamper the efficiency of the proposed wave-tracking method. A more intelligent subdomain assignment should rely on an adaptive strategy, based on a priori, physics-based knowledge and/or a posteriori error estimation.
Four frequency regimes were considered in this study: $ka = 1$ and $ka = 2$ (low-frequency), $ka = 5$ (resonance region), and $ka = 10$ (higher frequency). For comparison purposes, we also directly applied LSM and computed the relative error for these frequencies with variation of the mesh resolution, h/a, see Table 1. The performance of the two methods, LSM and LSM-WT, is assessed by determining the size of the corresponding linear system, N_ϕ, for a perscribed accuracy level (see Table 2). Moreover, since we use a direct method for solving the resulting linear systems, the number of nonzeros entries of the matrix $\mathbf{A}$, employed by both the LSM and LSM-WT, are reported in Table 2. Recall that this number is an indicator of factorization cost that complements the total number of unknown values.

The Pardiso direct solver, versions 4.1.0 - 4.1.2 [36, 37, 35, 38], was employed to solve the relatively large and sparse system given by Eq. (45), with multiple right-hand sides: Eqs. (46), (47), and (48). Solution of the comparatively smaller and dense Newton system Eq. (49) was completed by LU factorization with an in-house routine. The following numerical experiments were executed by a FORTRAN 90 code-base developed in this study, with parallel capability provided by the OpenMP application programming interface [30]. The program was run on the Lonestar and Blacklight supercomputing workstations supported by the Texas Advanced Computing Center and Pittsburghburgh Supercomputing Center respectively, as well as on a local AMD Opteron 4284 workstation with 128 GB of memory.

$(h/a)^{-1} \backslash\ ka$	1	2	5	10
32	10%			
40	9%	15%		
50	8%	14%		
64	7%	12%		
90		10%		
105		9%	28%	
160			23%	
200			20%	
300			17%	
600			12.3%	
800			11.2%	
925			10.2%	
1500			7.5%	21.7%
1700				20.7%
2000				19.5%

Table 1: Sensitivity of the relative error to the mesh refinement for four frequencies: ka = 1, 2, 5, and 10. Values report the total relative error of the scattered field approximated by LSM with 4 plane-waves per element.

	Relative	LSM			LSM-WT			
ka	Error	(h/a)	N_ϕ(x 10^3)	n_0 (x 10^6)	(h/a)	N_ϕ(x 10^3)	n_0 (x 10^6)	*iter.*
1	10%	1/32	16.4	0.327	1/6	0.576	0.011	3
2	10%	1/90	129.6	2.59	1/10	1.6	0.032	5
5	10%	1/925	13,690	271	1/50	40	0.798	13
5	5%	...	...	...	1/90	129.6	2.59	16
10	10%	...	...	...	1/160	409.6	8.19	20

Table 2: Comparison of the size of the global matrix **A** required to achieve a prescribed accuracy level for ka = 1, 2, 5, and 10, and 4 plane-waves per element. The total number of non-zero entries is listed as n_0. Missing LSM values were unattainable with 128 GB of memory.

5.1 Performance assessment for ka=1, ka=2

We set ka=1 and consider a discretization step size $h/a = 1/6$, that is, we define a mesh with 6 radial and 24 angular elements, i.e., N_h=144, as the total number of elements. The domain partition is comprised of 6 angular subdivisions, replicated in each quadrant in the manner depicted in Fig. 4. The basis functions are 4 plane-waves initially oriented parallel to the cartesian axes. As stated earlier, these plane-waves will be rotated by a common angle in radially aligned elements. Hence, the total number of unknowns (angles) in the Newton system is $N_\Omega = 6$. The obtained results are reported in Fig. 5, Fig. 6, and Tables 1 and 2. The following include observations and noteworthy points:

- Fig. 6 indicates that, at iteration 0, which corresponds to the plane-wave basis functions aligned parallel to the cartesian axes, the error is about 22%. This accuracy level delivered by LSM indicates that LSM-WT algorithm is applied very far from the pre-asymptotic convergence region. Yet, Fig. 6 and Table 2 show that LSM-WT converges after only 3 iterations to the prescribed accuracy level, %10 in the $\widehat{H^1}$-relative error over the computa-

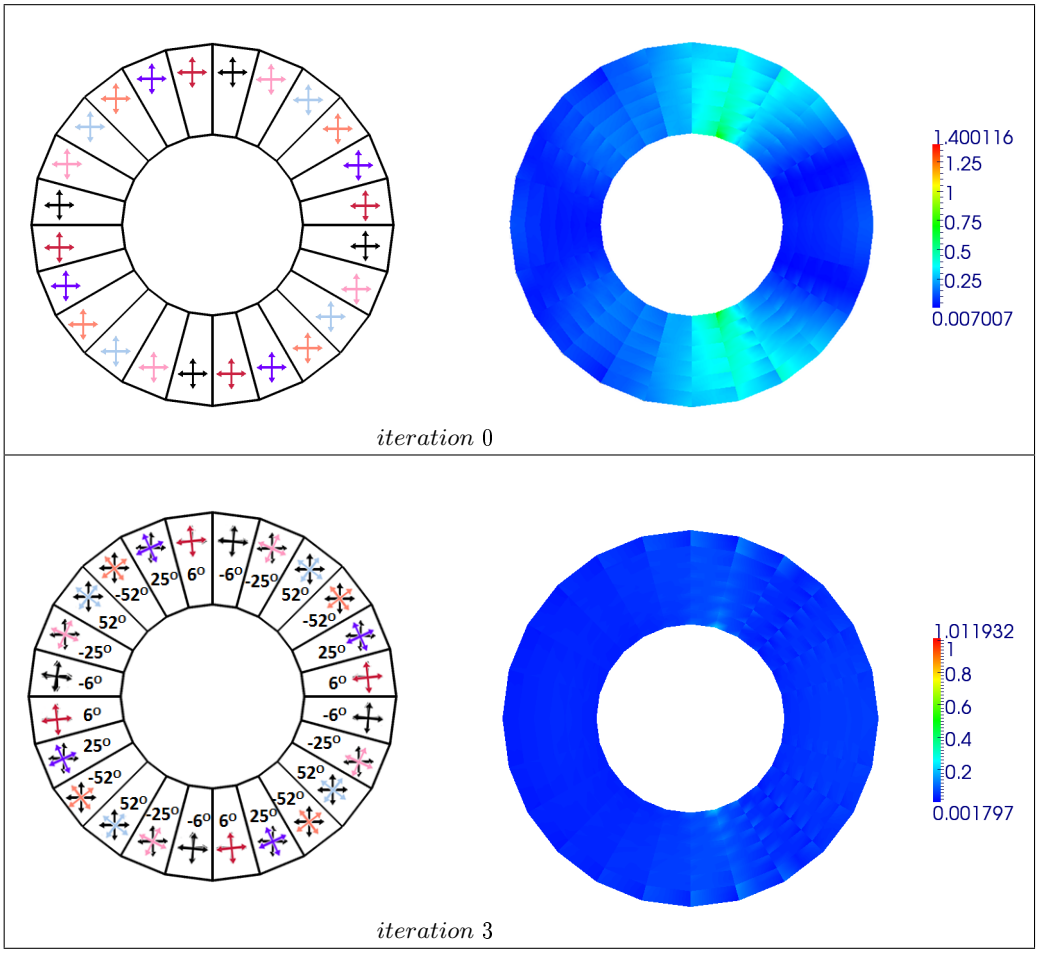

Figure 5: Plane-wave basis function orientation (left) and pointwise relative error of the absolute scattered field (right) for $ka = 1$, 4 plane-waves per element, h/a=1/6, $N_\Omega = 6$, and Newton iterations 0 and 3. The basis set orientation of all elements within a given subdomain are represented by their common value (left).

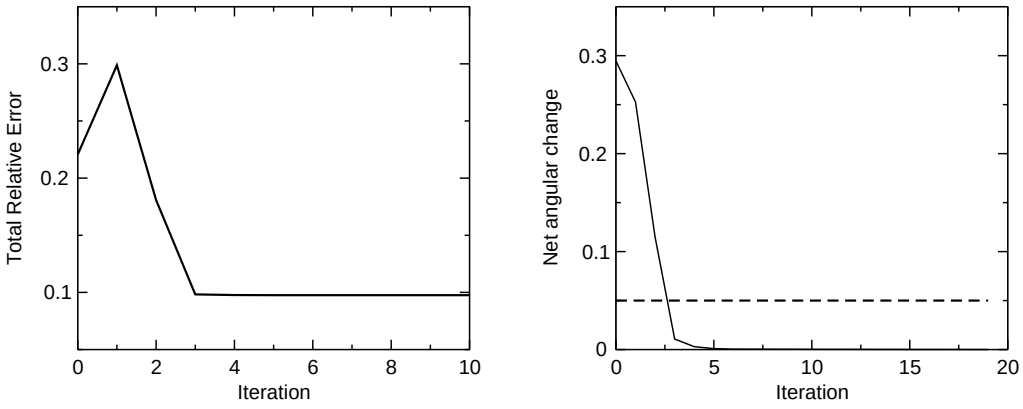

(a) (b)

Figure 6: Convergence history for ka=1, 4 plane-waves, h/a=1/6, and N_Ω=6. Total relative error (a) and relative change in the angles of the plane-waves (b), as a function of iteration (solid line). The specified convergence threshold is denoted by the dotted line (b).

tional domain.

- Fig. 5 reveals that the LSM-WT algorithm changed the orientation of the angles from their original positions by up to 52°counterclockwise and 25°clockwise, see Fig. 5, iteration 3. These individual rotations, demonstrate that it would be (a) improbable to predict such orientation combinations at iteration 0, and (b) computationally intractable for simpler combinatorial angle sweeping approaches to achieve such a level of accuracy.

- Fig. 6 describes the convergence history of the LSM-WT algorithm. As the minimization of the Newton system is a multi-variate problem it does not necessarily follow a path of monotonic decline, as evident by the peak in the first iteration in Fig. 6a. It is an attribute of the Newton method by which the system can "escape" local minima, although for any given iteration, the method may also overshoot optimal convergence parametrization. Rapid convergence is apparent by the monotonic decline in the relative error beginning at the second iteration. Fig. 6b also demonstrates that monitoring the relative successive change in the angle is a practical stopping criterion, with selection of 5% tolerance on this change is found to be suitable.

- Table 2 demonstrates the efficiency of the method. Specifically, achieving 10% of the $\widehat{H^1}$-relative error with 4 plane-waves per element requires a mesh size of $h/a = 1/32$ with LSM, whereas after 3 Newton iterations, LSM-WT converges to 10% error with a mesh size of $h/a = 1/6$. At each iteration, LSM-WT requires evaluation of one (576×576) linear system with 28 right-hand sides, in contrast to the comparative size of the LSM system: 16,400×16,400. Therefore, there is a reduction in both non-zero and total unknown values between LSM and LSM-WT by about a factor of 30.

- It should be acknowledged that LSM solves the system once, while at each Newton iteration, LSM-WT needs to build $\mathbf{A}$, multiple right-hand sides, and factor this system, which adds to computational cost. Note, the cost of building matrix $\mathbf{A}$ is significantly reduced by

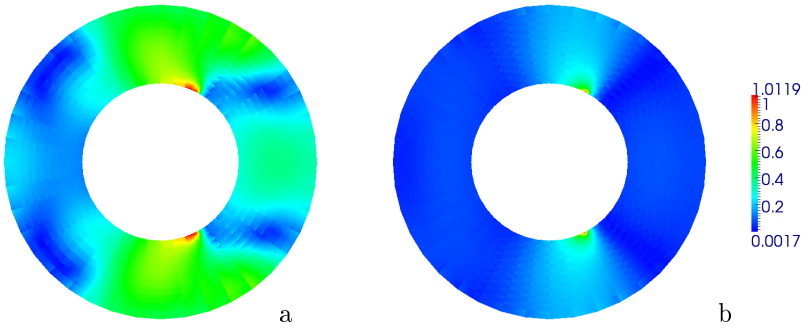

Figure 7: Error evaluation for the frequency ka=2, 4 plane-waves per element, h/a=1/10, and N_Ω=10. Pointwise relative error of the absolute scattered field for (a) LSM and (b) LSM-WT at iteration 5.

eschewing numerical quadrature, integration is evaluated analytically over the elemental edges (1D intersections). This significantly reduces the computational cost associated with building these matrices. The same observation applies to the construction of the right-hand sides. The cost for solving the Newton system is marginal as its corresponding matrix $\mathbf{M}^{(m)}$ is a 6 x 6 matrix. Thus, the competing factors, the size of the system and the number of iterations required to achieve target accuracy, govern computational efficiency. Due, in part, to the fact that construction and solution of additional right-hand sides do not significantly lengthen computational time, it is expected that the cost generated by multiple iterations becomes progressively attenuated as the size increases for larger systems incurred by standard LSM.

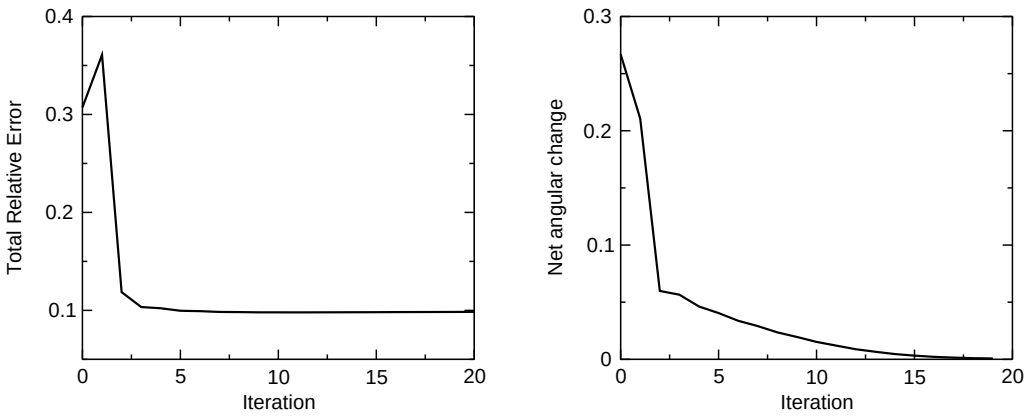

Figure 8: Convergence history for ka=2, 4 plane-waves, h/a=1/10, and N_Ω=10. Total relative error (a) and relative change in the angles of the plane-waves (b), as a function of iteration.

In the following results, the frequency is doubled, i.e., ka=2, while maintaining 4 plane-waves per element. We set the discretization step size $h/a = 1/10$, that is, we define a mesh with 10 radial and 40 angular elements, i.e., N_h=400, as the total number of elements. The domain partition is comprised of 10 angular subdivisions, replicated in each quadrant, i.e., N_Ω=10, as the total number of subdomains. Results are shown in Figs. 7, 8, and Tables 2 and 1. The following observations were taken:

- Fig. 8 indicates that, at iteration 0, which corresponds to the plane-wave basis functions aligned parallel to the cartesian axes, the error is about 31%. This accuracy level delivered by LSM indicates that LSM-WT algorithm is applied very far from the pre-asymptotic convergence region. Yet, Fig. 8 and Table 2 show that LSM-WT converges after only 5 iterations to the prescribed accuracy level, %10 in the $\widehat{H^1}$-relative error over the computational domain.
- Table 2 demonstrates the efficiency of the method. Specifically, achieving 10% of the $\widehat{H^1}$-relative error with 4 plane-waves per element requires a mesh size of $h/a = 1/90$ with LSM, whereas after 5 Newton iterations, LSM-WT converges to 10% error with a mesh size of $h/a = 1/10$. At each iteration, LSM-WT requires evaluation of one (1,600×1,600) linear system with 66 right-hand sides, in contrast to the comparative size of the LSM system: 129,600×129,600. Therefore, there is a reduction in both non-zero and total unknown values between LSM and LSM-WT by about a factor of 80. Note that the size of the Newton iteration matrix, $\mathbf{M}^{(m)}$, is only 10 x 10 and therefore its factorization is computationally negligible.
- Doubling the frequency required refining the mesh by a factor of 1.7 (h/a=1/6 for ka=1 and h/a=1/10 for ka=2). However, the number of iterations increased from 3 to 5 for $ka = 1$ to $ka = 2$. Nevertheless, the increased number of iterations is compensated by the gain in reduction in system size: a factor of 80 for ka=2 versus a factor of 30 for ka=1.

5.2 Performance assessment for ka=5

In the following computational experiment, a frequency of ka=5 is considered, while maintaining 4 plane-waves per element. We set the discretization step size $h/a = 1/50$. Hence, the mesh possesses 50 radial and 200 angular elements, i.e., N_h=10,000, as the total number of elements. The domain partition is comprised of 50 angular subdivisions, replicated in each quadrant, i.e., N_Ω=50. Results are shown in Figs. 9, 10, and Tables 1 and 2. The following observations are noteworthy:

- Fig. 10 indicates that, at iteration 0, which corresponds to the plane-wave basis functions aligned parallel to the cartesian axes, the error is over 40% corresponding to the accuracy level delivered by LSM. Clearly, LSM-WT algorithm is starting from an initial setup that is completely deviated from the target. In spite of this unacceptably high initial level of error, the algorithm attains 10% of the $\widehat{H^1}$-relative error after 13 iterations, as reported in Fig. 8 and Table 2.
- Table 2 demonstrates the efficiency of the method. Specifically, achieving 10% of the $\widehat{H^1}$-relative error with 4 plane-waves per element requires a mesh size of $h/a = 1/925$ with LSM, whereas after 13 Newton iterations, LSM-WT converges to 10% error with a mesh size of $h/a = 1/50$. At each iteration, LSM-WT requires evaluation of one (40,000×40,000) linear system with 1,326 right-hand sides, in contrast to the comparative size of the LSM

system: 13,690,000×13,690,000. Therefore, there is a reduction in both non-zero and total unknown values between LSM and LSM-WT by about a factor of 350. Note that the size of the Newton iteration matrix, $\mathbf{M}^{(m)}$ is only 50 x 50 and therefore, the solution of the corresponding system marginally impacts the overall computational cost.

- The number of iterations, m, is increasing with the frequency. In this case, the algorithm converged after 13 iterations. Nevertheless, the increased number of iterations is compensated by the gain in reduction in system size of a factor of 350.

- While error reduction by iterative application of the wave-tracking process is apparent by inspection of the pointwise representation of the relative error over the entirety of the computational domain (Fig. 9), significant reduction can be achieved in the regions with the highest LSM error, namely regions at angles of approximately $\pi/4$ and -$\pi/4$, by use of an adaptive strategy for apportionment of elements into the subdomains.

- The error and angular change profiles obtained as a function of iteration (Fig. 10), reveal more oscillations in the first iterations than shown previously for the ka=1 and ka=2 calculations (Figs. 6 and 8). This is most likely due to the fact that the initial error of the Newton algorithm is above 40%, and therefore the state might proceed through multiple local minima. Nevertheless, after the fourth iteration the algorithm then exhibits monotonic convergence.

Proceeding further, we maintain the frequency at ka=5 and reduce the target error level to 5%. To this end, we employ again 4 plane-waves per element, but refine the mesh to 90 radial and 360 angular elements, i.e., $1/h = 1/90$. The domain was partitioned into 90 angular subdivisions, replicated in each quadrant, i.e., $N_\Omega = 90$. Results are shown in Figs. 11, 12, and Tables 1 and 2. The following observations are noteworthy:

- Fig. 12a indicates that, at iteration 0, which corresponds to the plane-wave basis functions aligned parallel to the cartesian axes, the error is 31% corresponding to the accuracy level delivered by LSM. Again, the LSM-WT algorithm is starting from an unacceptably high initial level of error. The algorithm, however, attains 5% of the $\widehat{H^1}$-relative error after 16 iterations, as reported in Fig. 12a and Table 2.

- Table 2 reveals that even with a very fine mesh corresponding to $h/a = 1/1500$, incurring solution of a system comprised of about 36 million unknowns, LSM delivers a relative error of about 7.5%. Refining the mesh further exceeded our computational capabilities and therefore the 5% error level is computationally untractable with LSM. On the other hand, LSM-WT delivers the 5% error level by solving, at each Newton iteration, (a) a linear system with about 130 thousand unknowns and 4,186 right-hand sides, and (b) a small Newton system with 90 unknowns.
  It is recognized that increasing the number of plane-waves, without refining the mesh, can indeed improve the accuracy as well as the computational cost of LSM, as indicated in [29]. However, the objective of the proposed approach is precisely to avoid the necessity to excessively increase the number of required basis functions, which can lead to the risk of the loss of their linear independence. Additionally, LSM-WT can even be more competitive if equipped with a higher number of plane-waves in the elemental basis set, provided that their linear independence is numerically preserved.

- Dividing the error level from 10% to 5% was accomplished with LSM-WT by refining the mesh by less than a factor of 2 and by almost doubling the number of unknown angles.

5.3 Performance assessment for ka=10

We consider here a frequency value of $ka = 10$ and 4 plane-waves per element. The target error level in this numerical experiment is 10%. We consider a discretization step size $h/a = 1/160$, that is, we define a mesh with 160 radial and 640 angular elements, i.e., N_h= 102,500 as the total number of elements. The domain partition is comprised of 160 angular subdivisions, replicated in each quadrant in the manner depicted in Fig. 4. The four basis functions are initially oriented parallel to the cartesian axes. The obtained results are reported in Fig. 13, Fig. 14, and Tables 1 and 2.

- Fig. 14 indicates that, at iteration 0, which corresponds to the plane-wave basis functions aligned parallel to the cartesian axes, the error is about 45%. This accuracy level delivered by LSM indicates that LSM-WT algorithm is starting from an initial configuration setup that is completely deviated from the pre-asymptotic region. In spite of this unacceptably high initial level of error, the algorithm attains 10% of the $\widehat{H^1}$-relative error after 20 iterations, as reported in Fig. 14a and Table 2.

- Table 2 reveals that even with a very fine mesh corresponding to $h/a = 1/2000$, incurring solution of a system comprised of about 64 million unknowns, LSM delivers a relative error of about 19.5%. Refining the mesh further exceeded our computational capabilities and therefore the 10% error level is computationally untractable with LSM. On the other hand, LSM-WT delivers the 10% error level by solving, at each Newton iteration, (a) a linear system with about 410 thousand unknowns and 13,041 right-hand sides, and (b) a small Newton system with 160 unknowns. Again, in practical terms, this calculation became feasible by application of the wave-tracking strategy only.
  As stated earlier, it is possible to improve the accuracy as well as the computational cost of LSM by increasing the number of plane-waves without refining the mesh. We must reemphasize that the objective of the proposed approach is to avoid the necessity to excessively increase the number of required basis functions, which can lead to the loss of linear independence, notwithstanding that near-linear dependencies may not occur at this frequency value and considered mesh.

6 Summary and Conclusion

We have proposed a wave-tracking strategy to be incorporated into solution methodologies that employ local plane-wave approximations. The key idea here is that each plane-wave basis set, within considered elements of the mesh partition, is individually or collectively rotated to best align one function of the set with the main local propagation direction of the field. The goal in doing this is to maintain a low number of plane-wave basis functions while preserving the accuracy level. Consequently, it is expected that the approach will improve computational efficiency by avoiding numerical instabilities that result from near-linear dependency that may occur from increasing the number of plane-waves.
The proposed approach leads to the solution of a double minimization problem, where the unknowns are not only the usual nodes of the scattered field, but also the main directions of propagation. The least-squares formulation suggested in [29], a prototypical plane-wave based method, is considered in this study to serve as a suitable underpinning to be used in conjunction with the wave-tracking approach and, in its standard form, as an evaluative benchmark. This resulting, modified method is termed in this study as LSM-WT. The Newton method is applied to solve the resulting non-linear system. Exact characterization of both the Jacobian and Hessian is established to ensure convergence, stability, and robustness of the Newton algorithm.

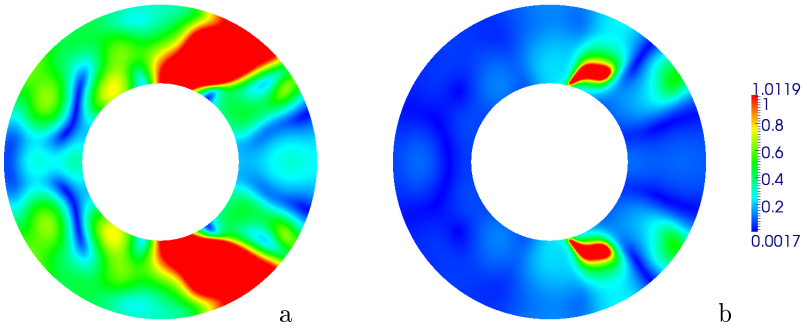

Figure 9: Error evaluation for the frequency ka=5, 4 plane-waves per element, h/a=1/50, and N_Ω=50. Pointwise relative error of the absolute scattered field for (a) LSM and (b) LSM-WT at iteration 13.

The computational effort for applying LSM-WT is predominately governed by the construction and factorization, at each Newton iteration, of the original least-squares scattering matrix, $\mathbf{A}$ with multiple right-hand sides. The matrix $\mathbf{A}$ is of dimension $N_\phi \times N_\phi$ (with N_ϕ defined as the total number of basis functions), and the number of right-hand sides is $\frac{1}{2}(N_\Omega + 1 \times N_\Omega + 2)$, where N_Ω is the number of distinct rotational angles considered. Subsequenty, a construction and factorization of a Newton matrix is required by the LSM-WT approach, however, the size of this system, $N_\Omega \times N_\Omega$ is much smaller than the scattering problem, i.e., $N_\Omega << N_\phi$.
An evaluation of the scattered field from a prototypical sound-hard, disk-shaped scatterer circumscribed by a Robin-type boundary, provided a model for assessment of LSM-WT evaluated with respect to conventional application of LSM. The results obtained from the numerical experiments, performed with 4 plane-waves, demonstrate: (a) the LSM-WT algorithm converges to the prescribed level of accuracy even when initiated from a configuration that deviates greatly from the pre-asymptotic region, (b) LSM-WT is shown to reduce the size of the LSM system by over two orders of magnitude depending on the frequency range, and (c) for higher frequency regimes and/or accuracy levels, LSM-WT allowed determination of the field, whereas application of LSM became computationally prohibitive.
Finally, it is anticipated that the performance of the LSM-WT approach can be improved by use of an adaptive strategy to intelligently partition the computational domain. This can be accomplished by an a posteriori error estimate that we have established. This estimate can be easily employed since it requires the computation of the the jumps of the scattered field over the interior element edges. Such values are, in practice, readily available as they are required for the construction of the matrix $\mathbf{A}$ corresponding to the direct scattering system.

7 Acknowledgment

The authors acknowledge the support by INRIA/CSUN Associate Team Program and the support of computational resources provided by the Extreme Science and Engineering Discovery Environment (XSEDE) program (grant No. DMS120018). Any opinions, findings, conclusions or recommendations expressed in this material are those of the authors and do not necessarily reflect the views of CSUN or INRIA.

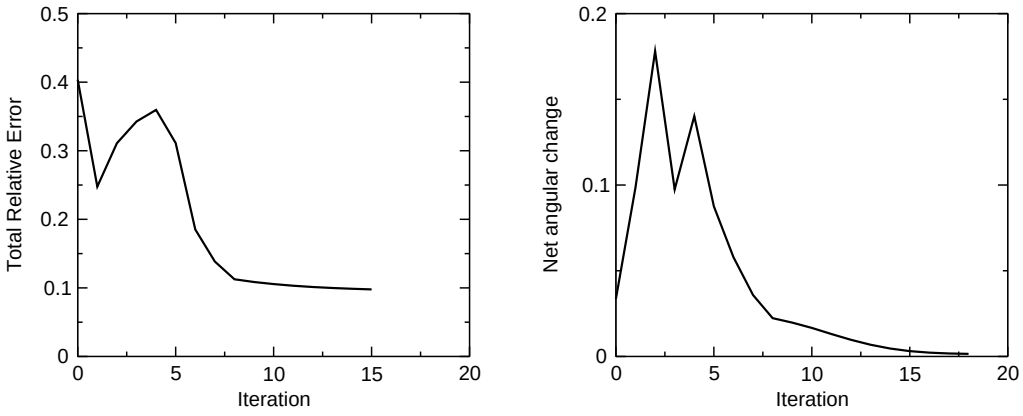

(a) (b)

Figure 10: Convergence history for ka=5, 4 plane-waves, h/a=1/50, and N_Ω=50. Total relative error (a) and relative change in the angles of the plane-waves (b), as a function of iteration.

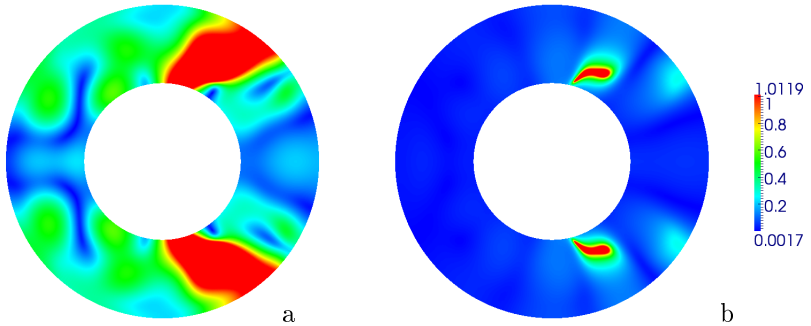

Figure 11: Error evaluation for the frequency ka=5, 4 plane-waves per element, h/a=1/90, and N_Ω=90. Pointwise relative error of the absolute scattered field for (a) LSM and (b) LSM-WT at iteration 16.

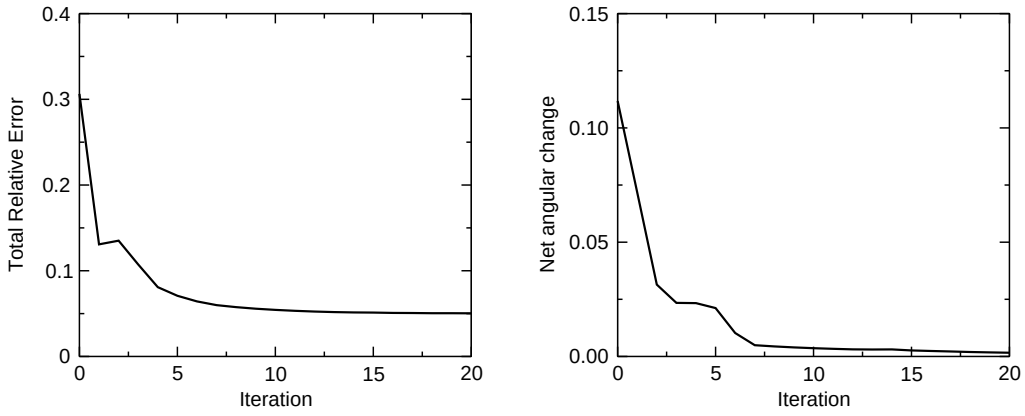

(a) (b)

Figure 12: Convergence history for ka=5, 4 plane-waves, h/a=1/90, and N_Ω=90. Total relative error (a) and relative change in the angles of the plane-waves (b), as a function of iteration.

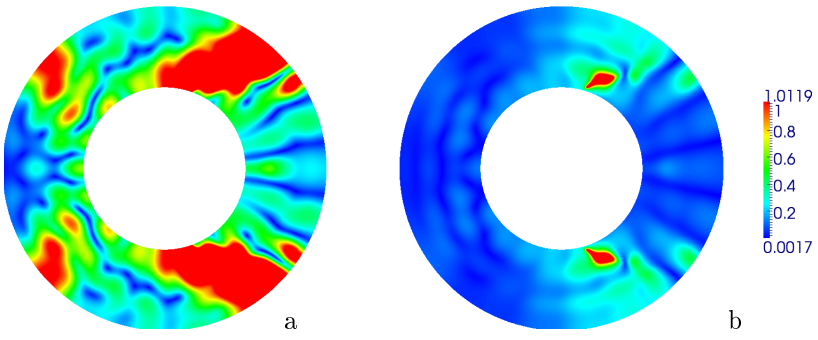

Figure 13: Error evaluation for the frequency ka=10, 4 plane-waves per element, h/a=1/160, and N_Ω=160. Pointwise relative error of the absolute scattered field for (a) LSM and (b) LSM-WT at 20 iterations.

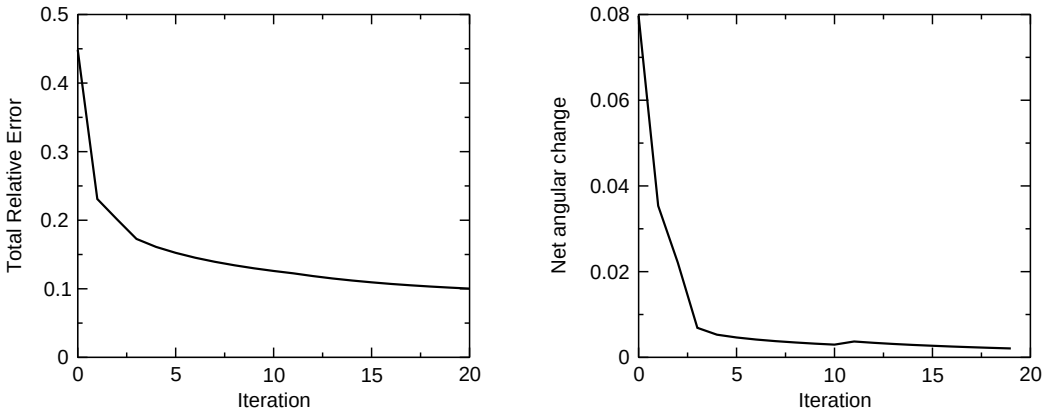

(a) (b)

Figure 14: Convergence history for ka=10, 4 plane-waves, h/a=1/160, and N_Ω=160. Total relative error (a) and relative change in the angles of the plane-waves (b), as a function of iteration.

References

[1] A. Ben-Menahem and S. J. Singh. Seismic Waves and Sources. Dover Publications, 2000.

[2] A. Walther. The Ray and Wave Theory of Lenses. Cambridge University Press, 1995.

[3] Mohamed Amara, Henri Calandra, Rabia Dejllouli, and Magdalena Grigoroscuta-Strugaru. A stable discontinuous galerkin-type method for solving efficiently helmholtz problems. Comput. Struct., 106 – 107:258 – 272, 2012.

[4] I. Babuška and I. Melenk. The partition of unity method. Int. J. Numer. Meth. Eng., 40:727 – 758, 1997.

[5] I. Babuška and S. Sauter. Is the Pollution Effect of the FEM Avoidable for the Helmholtz Equation Considering High Wave Numbers? SIAM J. Numer. Anal., 34:2392 – 2423, 1997.

[6] J.J. Bowman, T.B.A. Senior, P.L.E. Uslenghi, and J.S. Asvestas. Electromagnetic and acoustic scattering by simple shapes. North-Holland Pub. Co., 1970.

[7] D. Burnett. Radiation boundary conditions for the Helmholtz equation for ellipsoidal, prolate spheroidal, oblate spheroidal and spherical domain boundaries. J. Comp. Acous., 20:1230001, 2012.

[8] O. Cessenat and Després. Application of an ultra-weak variational formulation of elliptic PDEs to the two-dimensional Helmholtz problems. SIAM J. Numer. Anal., 35:255 – 299, 1998.

[9] S. Chaudhry. Efficient Solution Methodology Based on a Local Wave Tracking Strategy for Mid- and High-Frequency Helmholtz Problems. Master's thesis, California State University, Northridge, 2013.

[10] D. Colton and R. Kress. Inverse Acoustic and Electromagnetic Scattering Theory. Springer-Verlag, 1992.

[11] D. E. Goldberg. Genetic Algorithms in Search, Optimization, and Machine Learning. Addison-Weasley Professional, 1989.

[12] W. Desmet, P. van Hal, P. Sas, and D. Vandepitte. A computationally efficient prediction technique for the steady-state dynamic analysis of coupled vibro-acoustic systems. Adv. Eng. Softw., 33:527 – 540, 2002.

[13] F. Ihlenburg. Finite Element Analysis of Acoustic Scattering. Applied Mathematical Sciences. Springer-Verlag, 1998.

[14] F. Le Chevalier. Principles of Radar and Sonar Signal Processing. Artech House Publishers, 2002.

[15] Charbel Farhat, Isaac Harari, and Ulrich Hetmaniuk. A discontinuous Galerkin method with Lagrange multipliers for the solution of Helmholtz problems in the mid-frequency regime. Computer Methods in Applied Mechanics and Engineering, 192(11-12):1389 – 1419, 2003.

[16] Charbel Farhat, Radek Tezaur, and Paul Weidemann-Goiran. Higher-order extensions of a discontinuous galerkin method for mid-frequency helmholtz problems. International Journal for Numerical Methods in Engineering, 61(11):1938–1956, 2004.

[17] Charbel Farhat, Paul Wiedemann-Goiran, and Radek Tezaur. A discontinuous galerkin method with plane waves and lagrange multipliers for the solution of short wave exterior helmholtz problems on unstructured meshes. Wave Motion, 39(4):307 – 317, 2004.

[18] X. Feng and H. Wu. Discontinuous Galerkin methods for the Helmholtz equation with large wave number. SIAM J. Numer. Anal., 47:2872 – 2896, 2009.

[19] Xiaobing Feng and Haijun Wu. Discontinuous galerkin methods for the helmholtz equation with large wave number. SIAM J. Numer. Anal., 47(4):2872–2896, August 2009.

[20] Xiaobing Feng and Yulong Xing. Absolutely stable local discontinuous galerkin methods for the helmholtz equation with large wave number, 2010.

[21] B. Genechten, B. Bergen, D. Vanderpitte, and W. Desmet. A Trefftz-based numerical modeling framework for Helmholtz problems with complex multiple-scatterer configurations. J. Comput. Phys., 229:6623 – 6643, 2010.

[22] C. Gittelson, R. Hiptmair, and I. Perugia. Plane wave discontinuous Galerkin methods. ESAIM, Math. Model. Numer. Anal., 43:297 – 331, 2009.

[23] G. H. Golub and C. F. Van Loan. Matrix computations (3rd ed.). Johns Hopkins University Press, 1996.

[24] M. Grigoroscuta-Strugaru. Contribution à la résolution numerique des problèmes de Helmholtz. PhD thesis, L'Université de Pau et des Pays del'Adour, 2009.

[25] U. Hetmaniuk. Stability estimates for a class of Helmholtz problems. Commun. Math., Sci., 5:665 – 678, 2007.

[26] R. Hiptmair, A. Moiola, and I. Perugia. Approximation by plane waves. Seminar for Applied Mathematics, ETH Zürich, , 2009. Technical Report 2009-27.

[27] R. Hiptmair, A. Moiola, and I. Perugia. Plane wave discontinuous Galerkin methods for the 2D Helmholtz equation: analysis of the p-version. Seminar for Applied Mathematics, ETH Zürich, , 2009. Technical Report:2009-20.

[28] J. L. Lions and E. Magenes. Non-homogeneous Boundary Value Poblems and Applications, volume I. Springer-Verlag, 1972.

[29] P. Monk and D. Q. Wang. A least-squares method for the Helmholtz equation. Comput. Meths. Appl. Mech. Engrg., 175:121 – 136, 1999.

[30] OpenMP Architecture Review Board. OpenMP application program interface version 3.1, 2011.

[31] P. G. Ciarlet. The finite element method for elliptic problems. North Holland, Amsterdam, 1978.

[32] P. Grisvard. The finite element method for elliptic problems. Springer-Verlag, 1992.

[33] P. K. Kythe. An Introduction to Boundary Element Methods. CRC-Press, 1995.

[34] M. Rose. Weak element approximations to elliptic differential equations. Numer. Math., 24:185 – 204, 1975.

[35] O. Schenk, M. Bollhoefer, and R. Roemer. On large-scale diagonalization techniques for the Anderson model of localization. SIAM Review, 50:91 – 112, 2008.

[36] O. Schenk and K. Gärtner. Solving Unsymmetric Sparse Systems of Linear Equations with PARDISO. Future Gener. Comp. Sy., 20:475 – 487, 2004.

[37] O. Schenk and K. Gärtner. On fast factorization pivoting methods for symmetric indefinite systems. Elec. Trans. Numer. Anal., 23:158 – 179, 2006.

[38] O. Schenk, A. Waechter, and M. Hagemann. Matching-based Preprocessing Algorithms to the Solution of Saddle-Point Problems in Large-Scale Nonconvex Interior-Point Optimization. Comput. Optim. Appl., 36:321 – 341, 2007.

[39] E. Turkel. Boundary conditions and iterative schemes for the Helmholtz equation in unbounded regions. In F. Magoulés, editor, Computational Methods for Acoustic Problems , pages 127–158. Saxe-Coburg Publications, 2009.

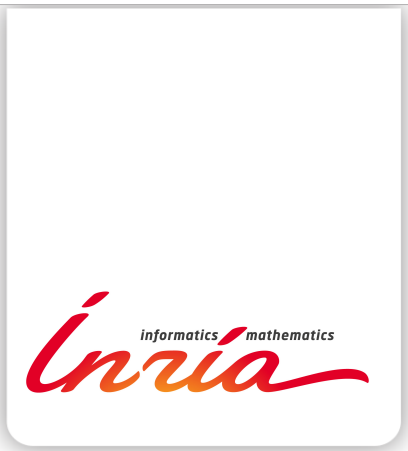

RESEARCH CENTRE
BORDEAUX – SUD-OUEST

200 avenue de la Vieille Tour
33405 Talence Cedex

Publisher
Inria
Domaine de Voluceau - Rocquencourt
BP 105 - 78153 Le Chesnay Cedex
inria.fr

ISSN 0249-6399